E&G Quaternary Sci. J., 68, 215–236, 2020
https://doi.org/10.5194/egqsj-68-215-2020

Open Access E&G Quaternary Science Journal

Research article

Sediment-filled karst depressions and *riyad* – key archaeological environments of south Qatar

Max Engel[1,2], Stefanie Rückmann[1], Philipp Drechsler[3], Dominik Brill[1], Stephan Opitz[1], Jörg W. Fassbinder[4,5], Anna Pint[1], Kim Peis[1], Dennis Wolf[1], Christoph Gerber[6], Kristina Pfeiffer[7], Ricardo Eichmann[7], and Helmut Brückner[1]

[1]Institute of Geography, University of Cologne, 50674 Cologne, Germany
[2]Geological Survey of Belgium, OD Earth and History of Life, Royal Belgian Institute of Natural Sciences, 1000 Brussels, Belgium
[3]Section for Early Prehistory and Quaternary Ecology, University of Tübingen, 72070 Tübingen, Germany
[4]Geophysics Section, Department of Earth and Environmental Sciences, Ludwig Maximilian University of Munich, 80333 Munich, Germany
[5]Archaeological Prospection Section, Bavarian State Department for Monuments and Sites, 80539 Munich, Germany
[6]Institute of Prehistory, Protohistory and Near-Eastern Archaeology, University of Heidelberg, 69117 Heidelberg, Germany
[7]Orient Department, German Archaeological Institute (DAI), 14195 Berlin, Germany

Correspondence: Max Engel (max.engel@uni-koeln.de)

Relevant dates: Received: 1 April 2019 – Revised: 5 November 2019 – Accepted: 29 November 2019 – Published: 9 January 2020

How to cite: Engel, M., Rückmann, S., Drechsler, P., Brill, D., Opitz, S., Fassbinder, J. W., Pint, A., Peis, K., Wolf, D., Gerber, C., Pfeiffer, K., Eichmann, R., and Brückner, H.: Sediment-filled karst depressions and *riyad* – key archaeological environments of south Qatar, E&G Quaternary Sci. J., 68, 215–236, https://doi.org/10.5194/egqsj-68-215-2020, 2020.

Abstract: Systematic archaeological exploration of southern Qatar started in the 1950s. However, detailed local and regional data on climatic fluctuations and landscape changes during the Holocene, pivotal for understanding and reconstructing human–environment interactions, are still lacking. This contribution provides an overview on the variability of geomorphic environments of southern Qatar with a focus on depression landforms, which reveal a rich archaeological heritage ranging from Palaeolithic(?) and Early Neolithic times to the Modern era. Based on a detailed geomorphic mapping campaign, sediment cores and optically stimulated luminescence data, the dynamics of *riyad* (singular *rawdha*; shallow, small-scale, sediment-filled karst depressions clustering in the central southern peninsula) and the larger-scale Asaila depression near the western coast are studied in order to put archaeological discoveries into a wider environmental context. Geomorphic mapping of the Asaila basin shows a much greater geomorphic variability than documented in literature so far with relict signs of surface runoff. An 8 m long sediment core taken in the sabkha-type sand flats of the western basin reveals a continuous dominance of aeolian morphodynamics during the early to mid-Holocene. Mounds preserved by evaporite horizons representing capillarites originally grown in the vadose zone are a clear sign of groundwater-level drop after the sea-level highstand ca. 6000–4500 years ago. Deflation followed the lowering of the Stokes surface, leaving mounds where the relict capillarites were able to fixate and preserve the palaeo-surface. Abundant archaeological evidence of Early and Middle Neolithic occupation – the latter with a clear focus inside the central Asaila basin – indicate more favourable

living conditions than today. In contrast, the sediment record of the investigated *riyad* in the south is very shallow, younger and controlled by surface discharge, deflation and the constantly diminishing barchan dune cover in Qatar over the Middle and Late Holocene. The young age of the infill (ca. 1500 to 2000 years) explains the absence of findings older than the Late Islamic period. Indicators of current net deflation may relate to a decrease in surface runoff and sediment supply only in recent decades to centuries. In the future, geophysical prospection of the *riyad* may help to locate thicker sedimentary archives and the analysis of grain size distribution, micromorphology, phytoliths or even pollen spectra may enhance our understanding of the interplay of regional environmental changes and cultural history.

Kurzfassung:

Die systematische archäologische Erkundung des Südens der katarischen Halbinsel begann in den 1950er Jahren. Lokale und regionale Daten zu den die regionale Kulturentwicklung begleitenden klimatischen Schwankungen und Landschaftsveränderungen im Holozän fehlen allerdings weitgehend. Dieser Beitrag liefert einen Überblick über die geomorphologische Variabilität des südlichen Teils von Katar mit einem Schwerpunkt auf karstbürtigen Hohlformen, deren verhältnismäßig reiches archäologisches Erbe bis in das Paläolithikum(?)/Frühe Neolithikum zurückreicht. Basierend auf einer detaillierten geomorphologischen Kartierkampagne, Sedimentkernen und Altersdatierung mit Hilfe optisch stimulierter Lumineszenz erfolgt eine Rekonstruktion der Sedimentationsgeschichte der räumlich bedeutenden *Riyad* (Singular: *Rawdha*; flache, kleinskalige, sedimentgefüllte Karsthohlformen) und des größeren Beckens von Asaila in der Nähe der Westküste, um die während der vergangenen Dekaden getätigten archäologischen Funde und Erkenntnisse in einen erweiterten Umweltkontext einzuordnen. Die geomorphologische Kartierung des Asaila-Beckens zeigt eine weit größere Variabilität an Oberflächenformen als bisher in der Literatur dokumentiert, darunter auch deutliche Indikatoren für reliktischen Oberflächenabfluss. Während der 8 m lange Sedimentkern aus dem sabkhaähnlichen Bereich des westlichen Beckens eine kontinuierliche Dominanz der äolischen Morphodynamik über das frühe bis mittlere Holozän andeutet, sind die von kleinen hügelartigen Formen dominierten Bereiche durch reliktische, einst in der vadosen Zone gewachsene kapillare Evaporithorizonte fixiert worden. Dies ist ein deutliches Zeichen für vorherrschende Deflation seit dem Hochstand des Meeresspiegels (und des Grundwasserspiegels) vor ca. 6000–4500 Jahren. Zahlreiche früh- und mittelneolithische Streufunde – letztere mit einem klaren Schwerpunkt im zentralen Asaila-Becken – weisen auf günstigere Lebensbedingungen zu dieser Phase hin. Die sedimentäre Füllung der untersuchten *Riyad* ist deutlich flacher und jünger und wird durch Oberflächenabfluss, Deflation und die sukzessiv abnehmende Barchan-Dünenbedeckung in Katar während des Mittel- und Spätholozäns determiniert. Das junge Alter der Füllung (ca. 1500–2000 Jahre) erklärt das Fehlen archäologischer Funde, die älter als spätislamisch datieren. Indikatoren aktuell dominierender Deflation (lineare Korrasionsrillen, Mikro-Yardangs) sind mögliche Hinweise auf einen Rückgang von Oberflächenabfluss und Sedimenteintrag innerhalb der letzten Jahrzehnte bis wenigen Jahrhunderte. Eine geophysikalische Prospektion der *Riyad*, die die Lokalisierung möglichst mächtiger Sedimentpakete erlauben würde, in Kombination mit der Analyse von Korngrößenverteilung, Mikromorphologie, Phytolithen oder gar Pollenspektren, könnte in Zukunft Teil einer Strategie sein, hier detailliertere Daten zur Paläo-Umweltdynamik der zentralen Bereiche Katars zu generieren.

1 Introduction

Pioneering archaeological surveys and excavations in Qatar started more than 60 years ago (e.g. Glob, 1958; Kapel, 1967; de Cardi, 1978; Tixier, 1980; Inizan, 1988). During the last decade, these were supplemented by intensified interdisciplinary research on all phases of the peninsula's cultural heritage (e.g. Al-Naimi et al., 2011; Rees et al., 2011; Cuttler and Al-Naimi, 2013; Eichmann et al., 2014; Gerber et al., 2014; Drechsler, 2014; Drechsler et al., 2013, 2016; Izquierdo Zamora et al., 2015; McPhillips et al., 2015). While evidence for the Palaeolithic remains under debate (Glob, 1958; Kapel, 1967; Al-Naimi et al., 2010; Cuttler and Al-Naimi, 2013; Scott-Jackson et al., 2015; Drechsler, 2014; Drechsler et al., 2016), Early and Middle Neolithic flint scatters along with burial cairns at a number of locations testify the occurrence of mobile to semi-stationary groups at that time (Drechsler et al., 2016). The Early Neolithic mainly comprises Qatar-B sites sensu Kapel (1967) and In-

izan (1988), tentatively dated to the 7th millennium BCE. The Middle Neolithic is often represented by surface finds of tile knives, scrapers, bifacial arrowheads and, in some cases, Ubaid-style pottery (Tixier, 1980; Inizan, 1988; Drechsler, 2014), which implies links with other Ubaid-related sites of the southern Arabian Gulf coast dated to the 6th–5th millennium BCE (Oates, 1978; Uerpmann and Uerpmann, 1996; Kainert and Drechsler, 2014). The earliest known settlement of Qatar was identified in Wadi Debayān at the northwest coast, dating back 7500 years (Al-Naimi et al., 2011; Tetlow et al., 2013). Of similar age are the fishermen's huts near Shagra at the east coast, which were associated with the Ubaid period by Inizan (1988). The decline of the Ubaid culture marked the onset of a period represented by very few cultural remains in Qatar, coinciding with the "Dark Millennium" as defined for the southeastern gulf shores (Uerpmann, 2003; Preston et al., 2012; Muhesen and Al-Naimi, 2014). The Bronze Age is only sparsely represented in Qatar, most prominently in the form of pottery and a purple-dye industry at Al-Khor north of Doha (Edens, 1999; Carter and Killick, 2010). Such finds are nearly absent in the southern part of the country (Gerber et al., 2014). Burial cairns are distributed over the entire peninsula and mostly from the Iron Age (ca. 300 BCE–300 CE) (Bibby, 1965; Buckley, 1973; Konishi et al., 1988), even though some of them have recently been dated to as old as the Ubaid period (Cuttler et al., 2013; Izquierdo Zamora et al., 2015). No evidence exists for Iron Age settlements, but a coexistence of nomadic pastoralism and sedentary lifestyles has been postulated (Muhasen and Al-Naimi, 2014). Permanent settlements emerged around the 8th century CE (Abbasid period), in particular along the northwestern coast (Guérin and Al-Naimi, 2009; Macumber, 2015). The nomadic and semi-nomadic Bedouin culture, however, coexisted and persisted well into the 20th century CE, focussing on the shallow karst depressions of the Qatar peninsula as campsites (McPhillips et al., 2015).

Underpinning research on the concomitant environmental changes is clearly in its infancy, consisting mainly of the outcome of the QNHER (Qatar National Historic Environment Record) project covering the northern part of the peninsula (e.g. Cuttler et al., 2011; Cuttler and Al-Naimi, 2013; Macumber, 2011, 2015; Tetlow et al., 2013). Isolated contributions to the framework of earlier archaeological missions mainly focus on Late Quaternary coastal changes and are rather preliminary (Vita-Finzi, 1978; Perthuisot, 1980). Thus, when the South Qatar Survey Project (SQSP) started in late 2012 as a joint operation between Qatar Museums and the Orient Department of the German Archaeological Institute, little well-established information existed regarding dynamics of vegetation, water availability and landforms. In the course of the archaeological survey, shallow, sediment-filled karst depressions referred to as *riyad* (singular *rawdha* or *rawdah*) (Batanouny, 1981; Babikir, 1986; Sadiq and Nasir, 2002; Al-Yousef, 2003; Macumber, 2011, 2015) turned out to be focal points of historic occupation, in contrast with the barren surrounding hamada (Eichmann et al., 2014; Gerber et al., 2014; Pfeiffer, 2015). A second priority of the SQSP was assigned to the large depression of Asaila in central-western Qatar (locally referred to as Jaow Al Bahath), which, compared to the rest of Qatar, preserves a high concentration of Early and Middle Neolithic single flint artefacts and flint artefact scatters, along with numerous findings of the pre-Islamic, Islamic and Modern periods (Kapel, 1967; Inizan, 1988; Pelegrin and Inizan, 2013; Drechsler, 2014; Drechsler et al., 2016).

This paper provides a general overview of the variability of geomorphic environments of southern Qatar (defined here as the part of the peninsula south of the Dukhan road; Fig. 1) over Holocene timescales. Based on a detailed geomorphic mapping campaign, sediment cores and optically stimulated luminescence (OSL) data, the dynamics of *riyad* and the basins of Asaila and adjacent Jaow Aqeeq (Fig. 1) are evaluated in order to put the Early Neolithic to Islamic archaeological discoveries of the SQSP (Drechsler, 2014; Drechsler et al., 2016; Eichmann et al., 2014; Gerber et al., 2014; Pfeiffer, 2015) into a wider environmental context.

2 The physical setting of southern Qatar

2.1 Geology and tectonic setting

The Qatar peninsula protrudes from the Arabian Peninsula into the Arabian Gulf. It represents an anticlinal structure of uplifted Palaeocene to Middle Eocene limestones, dolomites, marls, chalks and shales, intercalated with evaporites (Fig. 1). Lower and Middle Eocene carbonates comprise 80 % (Rus Formation $\sim$ 10 %; Dammam Formation $\sim$ 70 %) of Qatar's surface (Al-Yousef, 2003; Al-Saad, 2005). Miocene units are mainly found in southern Qatar, represented by the Dam and Hofuf formations. The Dam Formation consists of a sequence of shallow marine limestone, gypsum, dolomite and mud, whereas the Hofuf Formation also contains continental conglomerates with a matrix of aeolian sand and gypsum (Cavelier, 1970; Al-Yousef, 2003).

The topography is dominated by the central N–S-trending Qatar Anticline, which has been driven by tectonic uplift since the Palaeogene and created smaller anticlinal and dome structures. The Dukhan Anticline (NNW–SSE) in the west is another major structural feature, bearing the largest oil reservoirs of the area, creating a steeper surface relief than the Qatar Anticline and causing slight tilting of the entire limestone sequence (Al-Yousef, 2003).

2.2 Terrestrial geomorphic environments

2.2.1 Hamadas

Notable topographic elevations occur only in the south, reaching 103 m a.s.l. (above mean sea level) at the highest point. The majority of the peninsula is flat and the most widespread landform is hamadas (Fig. S8 in the Supple-

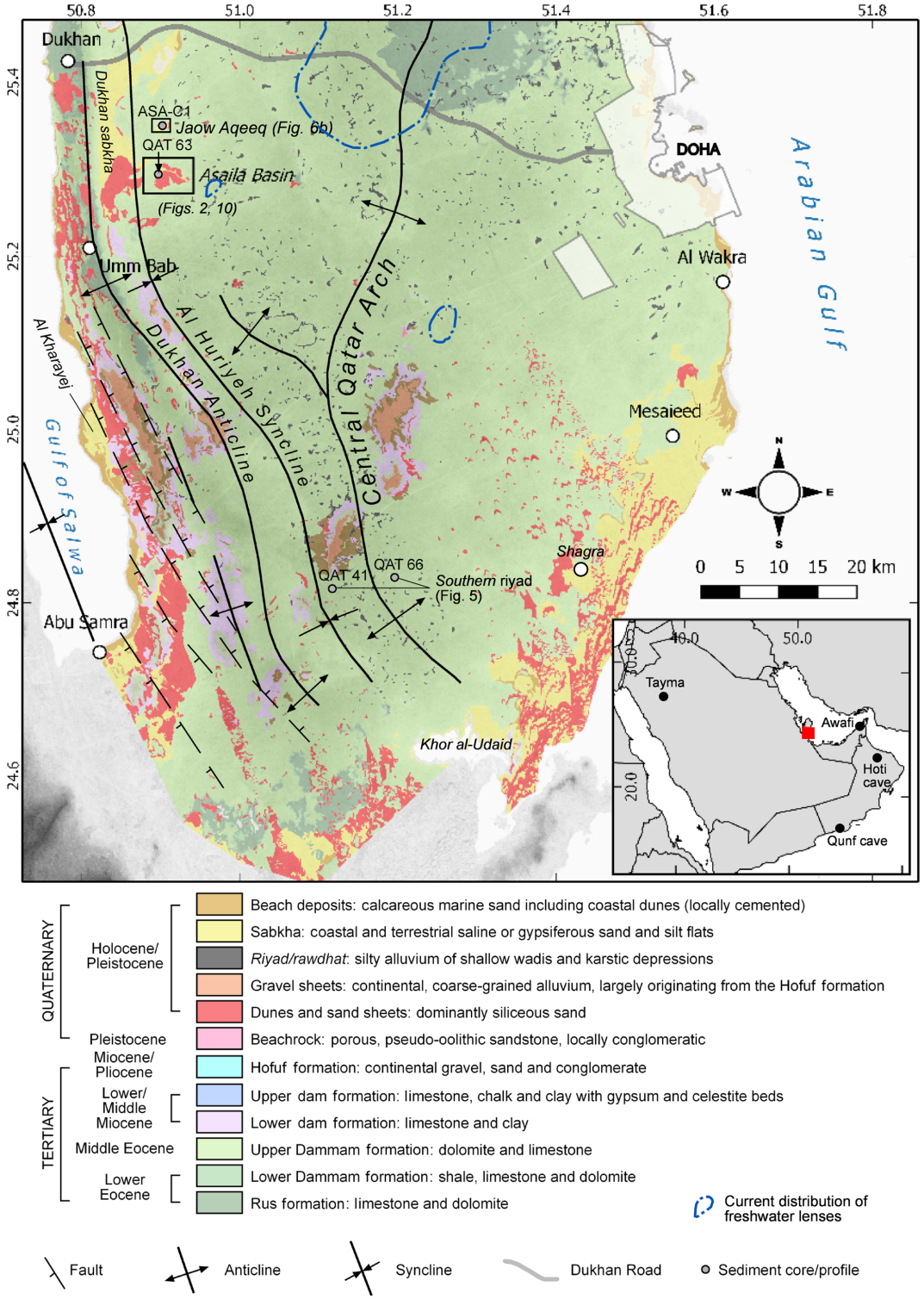

Figure 1. Geological map of southern Qatar based on the national geological map of 1980 (State of Qatar, 1980), overlying an ASTER global digital elevation model, which is a product of the US Ministry of Trade and Economy (METI) and the National Aeronautics and Space Administration (NASA). The main study area of the Asaila basin as well as coring sites in the Jaow Aqeeq basin further north (ASA-C1) and the southern *riyad* are depicted (QAT 41, QAT 66). Tectonic features are adapted from Al-Yousef (2003). The distribution of freshwater conditions in groundwater, which, depending on different sources, may have an upper limit of total dissolved solids of 3000 ppm (e.g. Heberger and Donnelly, 2015), are based on data of the Qatar Department of Environment, cited in Macumber (2012). The overview map indicates the location of the main map and palaeoclimate records referred to in the text.

ment), locally referred to as *hazm* (very gently sloping) or *mistah* (entirely flat), i.e. stone pavements covering most of the Dammam limestone province (Fig. 1) (Perthuisot, 1980; Batanouny, 1981). These plains are covered by mostly angular, in situ limestone gravel (see Benazzouz, 2004; Goudie, 2004b). Vegetation cover of the hamadas is very scarce; only isolated xerophile shrubs and trees such as *Tetraena qatarense*, *Acacia tortilis* or *Lycium shawii* are found between the surface stones (Batanouny, 1981).

2.2.2 Rocky ridges

Rocky ridges of southern Qatar relate to the N–S-trending anticlines, in particular to the Miocene Dam Formation along the southwest coast between Dukhan and south of Umm Bab (Fig. 1). They form mesas and buttes, controlled by varying resistivity of carbonate strata and reg surfaces, i.e. pavements of smaller, par-autochthonous clasts (see Benazzouz, 2004). Patchy sand accumulations in depressions of the rocky ridges are the only sites where sparse vegetation is found today, consisting mainly of *Panicum turgidum* and *Zygophyllum qatarense* (Fig. S14) (Batanouny, 1981).

2.2.3 Karst depressions

The term *rawdha* (Arabic "garden") refers to the fine-grained infill of shallow, round, slightly elongated or more irregular (e.g. when coalesced) inland depressions of 100 m up to a few kilometres in diameter. *Riyad* result from solution and collapse of the Eocene Rus and Dammam gypsum and limestone and are most abundant in the central part of the peninsula (Fig. 1). Their formation is related to the presence and orientation of anticlinal joints and fractures and, as hypothesized by Sadiq and Nasir (2002), to intensified karstification during the wetter Middle Pleistocene. *Riyad* sediments usually consist of light brown silty fine sand provided by sheet floods; carbonate and salt contents are low (Babikir, 1986). Usually they are topped by thin drapes of coarse aeolian sand or even nebkhas – mounds of aeolian sediment trapped and fixated by shrubs (Goudie, 2004a) – of up to 2 m height (Perthuisot, 1980; Macumber, 2011; Engel and Brückner, 2014). Most *riyad* are currently subject to deflation as indicated by micro-yardangs and linear corrasion features at the surface (Engel et al., 2018; Figs. S32, S33). The *riyad* of Qatar's interior provide evidence for occupation indicated by a considerable amount of pottery of different wares mostly dating into the (Late) Islamic and Modern periods. Stone structures of temporary character reflecting the presence of Bedouins are abundant (Eichmann et al., 2014; Gerber et al., 2014). The widest and deepest depressions of southern Qatar, significantly exceeding the dimensions of *riyad*, are the Asaila basin ("Acila depression" in Inizan, 1988; Macumber, 2012; Pelegrin and Inizan, 2013; local name is Jaow al Bahath), separated from the Dukhan continental sabkha by a massive limestone ridge, and the Jaow Aqeeq basin (Fig. 1). Both depressions result from collapse and solution over major faults and joint-flow drainage estimated to be active at least since the Miocene. Sadiq and Nasir (2002) suggest a genetic sequence reaching from deepening and widening cylindrical karst pits, which coalesce subterraneously (compound karst pits) and develop larger bottle- and bowl-shape karst pits through collapse processes. These pits gradually fill up with predominantly aeolian deposits to form such mature depressions or basins.

2.2.4 Wadis

Wadis are most prominent in the southwest of Qatar, where they accumulate some silt and clay and are intercalated by gravel sheets, which result from episodic rainfall events. The wadis show a relatively dense vegetation cover characterized by *Pennisetum divisum*, *Acacia ehrenbergiana*, *L. shawii* and, where aeolian dynamics increase, *Leptadenia pyrotechnica* (Batanouny, 1981).

2.2.5 Coastal sabkhas

The low-lying coastlines of Qatar support the formation of coastal sabkhas, i.e. saline flats in intertidal position. Coastal sabkhas are extensive in the southeast, around Khor al-Udaid, and are characterized by temporary flooding, a water table close to the surface and the precipitation of evaporites within the sediment column and on the surface. A large continental sabkha without surface connection to the sea is formed in the synclinal depression east of the Dukhan Ridge. Its lowest point is 6 m below sea level (Al-Yousef, 2003). The coastal sabkhas are Holocene features mostly resulting from coastal progradation along the entire Qatari coast following the mid-Holocene sea-level highstand (e.g. Billeaud et al., 2014; Strohmenger and Jameson, 2018). Coastal sabkhas with fine-grained soil may host halophile vegetation such as *Arthrocnemum glaucum*, *Juncus rigidus* or *Aeluropus lagopoides*. Where they merge into tidal flats not bordered by beach ridges, mangroves of *Avicennia* may establish (Batanouny, 1981).

2.2.6 Barchan dunes

In addition to the sand deposits found along the rocky ridges of southwestern Qatar, aeolian processes formed barchan dune fields in the southeast. The availability of quartz sand as source material and the regional Shamal wind system approaching from NW to NNW are the defining factors (Embabi and Ashour, 1993; Rao et al., 2001; Al Senafi and Anis, 2015). Once having crossed and covered the peninsula from NNW to SSE, the sediment source area towards the inner gulf became cut off due to the Holocene marine transgression into the Arabian Gulf, just before the mid-Holocene sea-level highstand. The southeastern dune population migrating with a speed of several metres per year represents a relict landform constantly diminishing in size as the dunes "calve"

into the Arabian Gulf (Engel et al., 2018). While the barchan dunes themselves are free of vegetation, *Cyperus conglomeratus* may establish along their margins (Batanouny, 1981).

2.3 Present and former climate

The present climate of Qatar is arid, though the relative humidity may rise up to 90 %. Annual rainfall amounts to 50–80 mm and mainly occurs during winter and spring. However, the spatio-temporal pattern of rainfall is highly irregular (Embabi and Ashour, 1993). The NW-to-NNW Shamal winds are active mostly during early June to mid-July and November to March (Rao et al., 2001; Al-Yousef, 2003; Al Senafi and Anis, 2015), and they drive aeolian morphodynamics throughout the peninsula (Embabi and Ashour, 1993; Engel et al., 2018).

Climate as the dominant factor shaping the physical landscape, controlling water availability and influencing occupation patterns of Qatar, has varied in the past. During glacial–interglacial cycles, and even on millennial timescales over the Holocene, geological records from different parts of the Arabian Peninsula indicate considerable fluctuations (e.g. Fleitmann et al., 2007; Engel et al., 2012, 2017; Preston et al., 2012; Dinies et al., 2015, 2016; Guagnin et al., 2016; Parker et al., 2016, Breeze et al., 2017; Parton et al., 2018). The closest palaeoclimate record on the Arabian Peninsula is located at Ras al-Khaimah, UAE (Preston et al., 2012; Parker et al., 2016), where lake deposits reflecting a rainfall surplus date between 9.0–8.3 and 3.0 ka cal BP. The only reference presenting local Late Quaternary rainfall variability of Qatar describes humid conditions during the Last Glacial Maximum 20 kyr ago and increasing aridity towards the present with a short humid deviation during the mid-Holocene. However, this curve has to be considered with caution since no specific data source is provided (Perthuisot, 1980).

As recharge rates are low, permanent freshwater bodies are absent. Easily accessible, potable groundwater aquifers representing the main limiting factor of ancient settlement activity are rare. Most freshwater aquifers occur in the north, while in the south they are very local and isolated (Fig. 1). Groundwater tables at the coast tend to incline towards the sea level. According to Macumber (2011, 2015), the Asaila depression is one of the few sites with relatively easy access to shallow fresh to slightly brackish groundwater in the south of Qatar.

3 Methods

This study is based on work carried out at the Asaila basin, the basin of Jaow Aqeeq and two specific *riyad* in the southern part of the peninsula (Fig. 1). At Asaila, we conducted a detailed geomorphic mapping campaign, carried out a magnetometer prospection and took an 8 m long sediment core (QAT 63). At Jaow Aqeeq, a 3 m long sediment core (ASA-C1) was taken in order to compare sedimentation patterns inside both basins with different hydrological conditions. The sediment infill of two *riyad* was investigated based on a trench (QAT 41) and a short sediment core (QAT 66).

3.1 Geomorphic mapping

To develop our understanding of past and present geomorphic processes shaping the Asaila depression, a detailed geomorphic mapping campaign was initiated to identify environmental controls of landscape dynamics and explain the spatial distribution of archaeological surface findings. Pre-existing mapping resources included a multispectral IKONOS mosaic from 2004 (resolution $\sim 1\,\mathrm{m\,pixel^{-1}}$), the geological map of Qatar (State of Qatar, 1980), the topographic map of Qatar (State of Qatar, 1971), a predecessor geomorphic map of Inizan (1988) and local geological maps of Al-Yousef (2003), which were used for an initial classification of landforms as polygons in ArcMap v10.3.1. A total of 2 weeks of field mapping in March 2016 included photographic documentation, verification and refinement of the existing documentation. Site location and topographic profiles were realized using a TOPCON Hiper Pro differential global navigation satellite system (DGNSS) with a lateral and vertical error of ± 2 cm, a manual GPS and a laser rangefinder (TruPulse 200, Laser Technology Inc.). The resulting map describes (i) geomorphic surface units based on the rock type and type of sediment deposit, (ii) morphodynamics and morphogenesis (aeolian, fluvial, etc.), and (iii) morphometry (slopes, microrelief). Vegetation within the depression was recorded and determined using Batanouny (1981) and Norton et al. (2009).

3.2 Magnetometer prospection

To verify the existence of former surface runoff patterns into the Asaila basin (see geomorphic map in Inizan, 1988) and to localize relict fluvial landforms, a magnetometer prospection was carried out in the area of the Acila 36 excavation (Inizan, 1988; Pelegrin and Inizan, 2013) in the northern part of the basin (Fig. 2). In order to reach the highest possible sensitivity, to realize a time-efficient prospection and to receive additional information on the enrichment of magnetic minerals in lateral sediment layers, we used the Cs total field magnetometer (Scintrex SM4G-Special) using the "duo-sensor" configuration (see examples in Fassbinder, 2015, 2017). Five adjacent grids of 40 m × 40 m were prospected. All details regarding the prospection and data analysis are presented in Supplement Sect. S1.

3.3 Sampling and survey of sediment archives

To study potential changes in depositional environments, which would have had essential implications for the interpretation of the survey findings, a vibracore (QAT 63) was taken in the western part of the Asaila basin using an Atlas Copco Cobra mk1 coring device and open steel probes of 6 and 5 cm

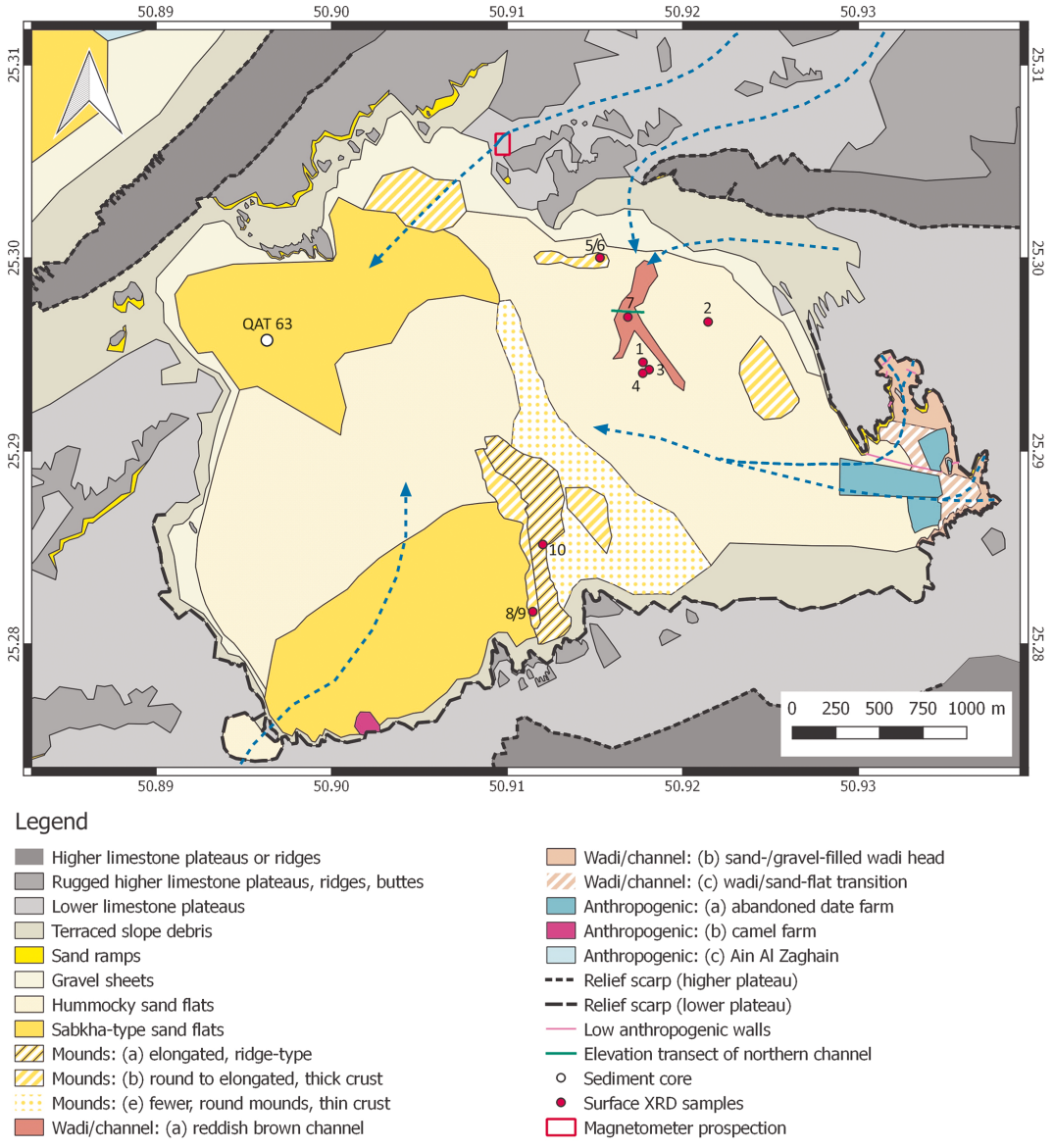

Figure 2. Geomorphic map of the Asaila basin indicating main pathways of surface water inflow (blue arrows; based on Inizan, 1988, and own landform interpretation) as well as the location of the elevation transect across the northern channel (Fig. 5), core QAT 63 (Fig. 6), surface XRD samples (Figs. S5–S7, Table S2) and the magnetogram (Fig. 4).

in diameter. A second shorter core (QAT 63 OSL) was taken at the same site using closed, opaque PVC liners in order to retrieve sample material for optically stimulated luminescence (OSL) dating (Drechsler et al., 2016). For comparison, we extended the analysis of sedimentary archives to the adjacent basin of Jaow Aqeeq, located seaward of the rocky ridge separating the Asaila depression from the Dukhan sabkha. Sediment core (ASA-C1) was taken in the northeastern part of the basin of Jaow Aqeeq (Fig. 1). In order to investigate the formation and dynamics of the key archaeological environments of the *riyad*, many were visited and described during the field surveys between 2012 and 2016, while two of them were studied in more detail using a sediment core (QAT 66) and a trench (QAT 41).

3.4 Sedimentary analyses and dating

3.4.1 Grain size analysis

Due to their overall coarse texture, samples of QAT 63 were analysed for grain size and grain shape by applying dynamic image analysis (Retsch Camsizer P4, particle size range of 30–30 000 µm). Samples from Jaow Aqeeq (ASA-C1) and the *riyad* (QAT 41, QAT 66) were measured using a laser particle analyser (Beckman Coulter LS 13320; particle size range of 0.04–2000 µm) because these had a significant silt

component. For analysis of the latter, the pre-treatment procedure includes air-drying of sample material, careful hand pestling and dry-sieving < 1 mm. H_2O_2 (15 %) was added to a < 1 mm aliquot of 0.2–1.0 g in order to remove organic carbon. The sample was washed using a centrifuge until a pH value of 6–8 was reached to avoid neutralization after the addition of 0.5N $Na_4P_2O_7$ (55.7 g L^{-1}) for aggregate dispersion. Calculation of statistical parameters was performed using the GRADISTAT statistic package (Blott and Pye, 2001).

3.4.2 X-ray diffraction analysis

Selected surface samples from the Asaila depression were subjected to X-ray diffraction (XRD) analysis using a Siemens D5000 powder diffractometer (Cu tube) to determine if the landforms are actively formed or of relict nature (active formation may be indicated by the presence of easily soluble evaporites). Samples were measured over a range of 5–75° (2θ) with a step size of 0.05° and a time of 4 s per step (aperture slit = 0.5). The diffractograms were analysed by employing the EVA software package and the ICDD (International Centre for Diffraction Data) database.

3.4.3 OSL dating

Due to a lack of material suitable for radiocarbon dating, age estimates for selected units in the Asaila depression and the *riyad* are derived from OSL dating of sand-sized quartz grains (see Sect. S2 and Figs. S1–S4 for details).

4 Results

4.1 Landforms of the Asaila basin

The Asaila basin has an extent of ca. 12 km^2. It is mostly closed, apart from its western margin, where it is connected with the southwestern extension of the Dukhan sabkha through a series of ridges and small depressions. Detailed field mapping revealed a surprisingly wide range of landform units (Fig. 2; see Sect. S4 for detailed explanations), some of which clearly relate to the former presence of surface water and were probably formed by surface processes during the Holocene.

The basin is framed by the flint-bearing limestone plateaus of the Dammam Formation, consisting of two clear plateau levels, i.e. the higher limestone plateau (ca. 13–18 m Qatar National Datum, QVD), including the rugged higher limestone plateau along its basinward transition (ca. 8–15 m QVD) and the lower limestone plateau (ca. 2–8 m QVD). The higher limestone plateau forms a massive NE–SW-trending structural landform and separates the Asaila basin from the adjacent Dukhan sabkha. Another unit of the higher limestone plateau bounds the basin in the northeast. The transition from the lower limestone plateau to the floor of the Asaila basin occurs quite abruptly in the southwest, south and east, in the form of a vertical step (Fig. 3a). In the north and northwest, the transition is relatively smooth with broad units of terraced slope debris and sand-and-gravel sheets (Figs. 2, 3a). In the northernmost part of the basin, where the lower limestone plateau merges into the gravel sheet, the excavation Acila 36 of Inizan (1988) and Pelegrin and Inizan (2013) is located. At this type site for the Middle Neolithic Qatar-B industries, a new magnetometer prospection was carried out (Fig. S13). Despite poor magnetic susceptibility of the loose sediment cover due to low heavy mineral and iron oxide contents and internal magnetization contrasts of only ±0.8 nT, an unequivocal 10–15 m wide channel structure covered by sand and gravel and running towards the basin can be inferred (Fig. 4). The finding corroborates the assumption of Inizan (1988) of a major inactive surface water trajectory into the basin in this area (Fig. 2). Other geomorphic features reflecting more recent fluvial activity include the following:

i. The first feature is a broad, vegetation-free, linear surface depression of 10–20 cm depth (Fig. 5) with a weak, reddish-brown surface crust of gypsum, quartz sand and calcite (Fig. S6, Table S2) as well as high amounts of clay and silt (Fig. S31). It extends from the central northern margin and bifurcates towards the centre of the basin (Fig. 2).

ii. The second feature is a wadi channel at the eastern end of the Asaila basin, characterized by retrogressive erosion (Figs. S29, S30). The wadi is filled with slope debris and experiences aeolian overprinting in the form of sand ramps (Figs. S12, S29a). However, horizontally bedded platy clasts in a poorly sorted, consolidated sandy matrix and an outwash channel exposing barren bedrock point to at least episodic surface water flows in recent times (Figs. S29a, S30a).

The most extensive landform unit inside the Asaila basin is the hummocky sand flats (Fig. 2), which mostly comprise nebkha fields originating from *Zygophyllum qatarense* shrubs. Some of the nebkhas seem inactive and are protected by thin evaporitic crusts made of gypsum, calcite and minor amounts of sylvine, mixed with quartz sand (samples ASA 1 and 2; Fig. S5, Table S2). In some areas, even halite was present (ASA 3; Fig. S5, Table S2).

Some areas in the central southern, northern and eastern parts are densely covered by characteristic mounds significantly higher than the nebkhas. They are fixated and protected by evaporitic horizons of massive to porous gypsum and minor amounts of calcite and sylvine (samples ASA 5, 6, 8–10; Figs. 3b, S6, S7, Table S2). These mounds vary from perfectly round, up to 1 m high, to narrow, cross-cutting ridges, several tens of metres long (Fig. 3b). Furthermore, large parts inside the basin are covered by vegetation-free sabkha-type sand flats (Fig. 3a, b) with gypsum- and halite-containing surface crusts, in some parts even polygonal structures (Figs. S19, S20).

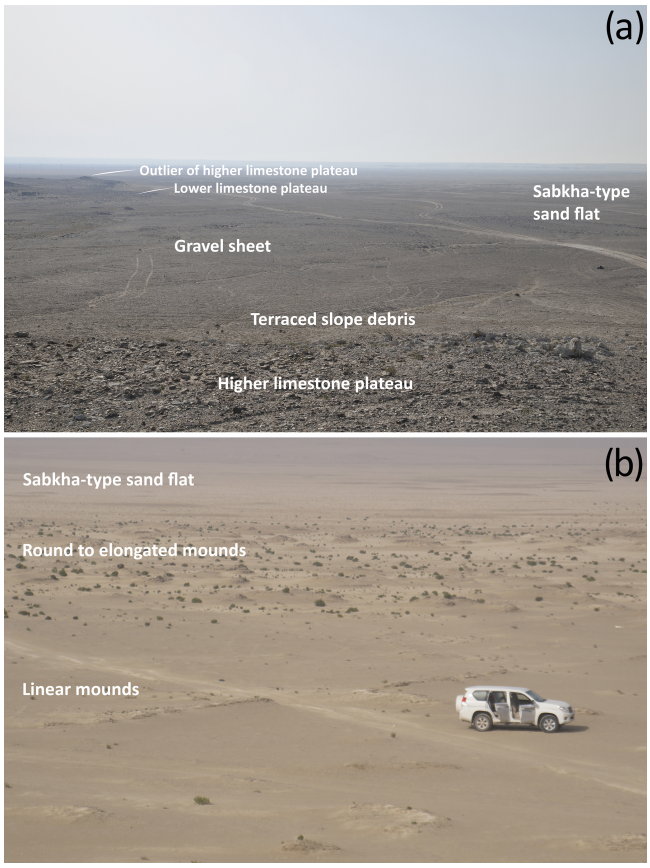

Figure 3. **(a)** View into the Asaila basin from the higher limestone plateau of the NE edge directed towards the east. It shows the terraced slope debris and the gravel sheet merging into the sabkha-type sand flat. In the background, the innermost outlier of the higher limestone plateau is visible, resting on top of the lower limestone plateau. **(b)** View into the basin from an outlier of the rugged higher limestone plateau of the central southern rim directed towards the west. It shows the linear, almost vegetation-free mounds in the foreground, followed by the elongated to round mounds with denser vegetation and the vegetation-less sabkha-type sand flat of the western basin.

4.2 Sedimentary infill of the Asaila depression

Sediment core QAT 63 was taken in the low-lying sabkha-type sand flats of the northwestern Asaila basin (Figs. 2, S21). It reached a depth of 8 m and consists of moderately sorted to moderately well-sorted fine to very fine gravelly medium sand (sensu Blott and Pye, 2001) (Fig. 6). Despite the slight variation in fine, medium and coarse sand, no facies changes occur. Grain size distributions are generally symmetrical to slightly coarsely skewed, apart from samples at 0.58–0.50 m below surface (b.s.) and ca. 1.55–1.40 m b.s., which are very coarsely skewed and poorly sorted. These samples, along with the surface sample, also have the lowest value for grain sphericity and width to length ratio of the entire sequence. A trench next to QAT 63 revealed a massive subsurface gypsum crust at 0.60–0.50 m b.s., while the overlying sands are clearly cross-bedded (Fig. 6b).

Three samples were taken for OSL dating at 0.40 (small trench), 1.90–1.60 and 2.90–2.60 m b.s. (both from core QAT 63 OSL). They reveal coarse-grain (150–200 µm) quartz ages of 5800 ± 300, $6400 \pm 300 - -7300 \pm 300$, and 7500 ± 300 years, respectively (Fig. 6, Table S1). While for the uppermost sample right above the gypsum crust the measured water content of 7 % was used for age calculation, two ages were generated for the sample 1.90–160 m b.s., which is probably located in the vertical fluctuation range of the local groundwater table. The younger age implies a water content of 10 % as measured in the laboratory, the older one assumes water saturation. While fluctuating water contents over time introduce dating uncertainties, the overdispersion of the rather symmetric equivalent dose distributions of 8 %–15 % suggests that incomplete signal resetting is not an issue (Fig. S4).

4.3 The depression of Jaow Aqeeq

Jaow Aqeeq is another larger-scale topographic depression north of Asaila, located close to the coastal sabkha of Dukhan and seaward of the SW–NE-trending limestone ridge separating Asaila from the Dukhan sabkha (Figs. 1, S32). Both depressions share strong geomorphic similarities, even though traces of surface runoff are more prevalent in Jaow Aqeeq compared to Asaila. Outside the depression along its eastern margin, a wide range of archaeological surface finds include fireplaces, clusters of pottery sherds and lithic artefacts (flakes, blade tools, arrowheads), cairns, shells, coins, metal pieces, bulbs of flint, remains of a provisional mosque, and several modern structures. Some of the lithic artefacts may correspond to the Early Neolithic Qatar-B industry, but the context is largely undated. Multiphase utilization of the site is evident. Distinct areas of domestic use and associated lithic workshops (later overprinted by cairns) as well as mosques and modern structures have been mapped (Fig. 7b). The record inside the basin is very poor so far, only consisting of modern garbage (Schönicke et al., 2016). The surface of the inner depression reveals higher moisture and higher abundance of halite- and gypsum-dominated crusts as compared with the Asaila basin.

In order to improve our understanding of the differences between Asaila and nearby Jaow Aqeeq and to evaluate sediment infill, hydrological conditions and palaeoenvironmental changes, sediment core ASA-C1 was taken inside the Jaow Aqeeq depression close to a temporary shallow standing waterbody (Figs. 7, S32). At the surface, the buckled gypsum crust, several centimetres thick and in some places thinly covered by white halite crystals, appeared very similar to sabkhas along the coast of southwest Qatar (e.g. Dukhan sabkha; Al-Yousef, 2003). The groundwater table was located at 35 cm b.s.

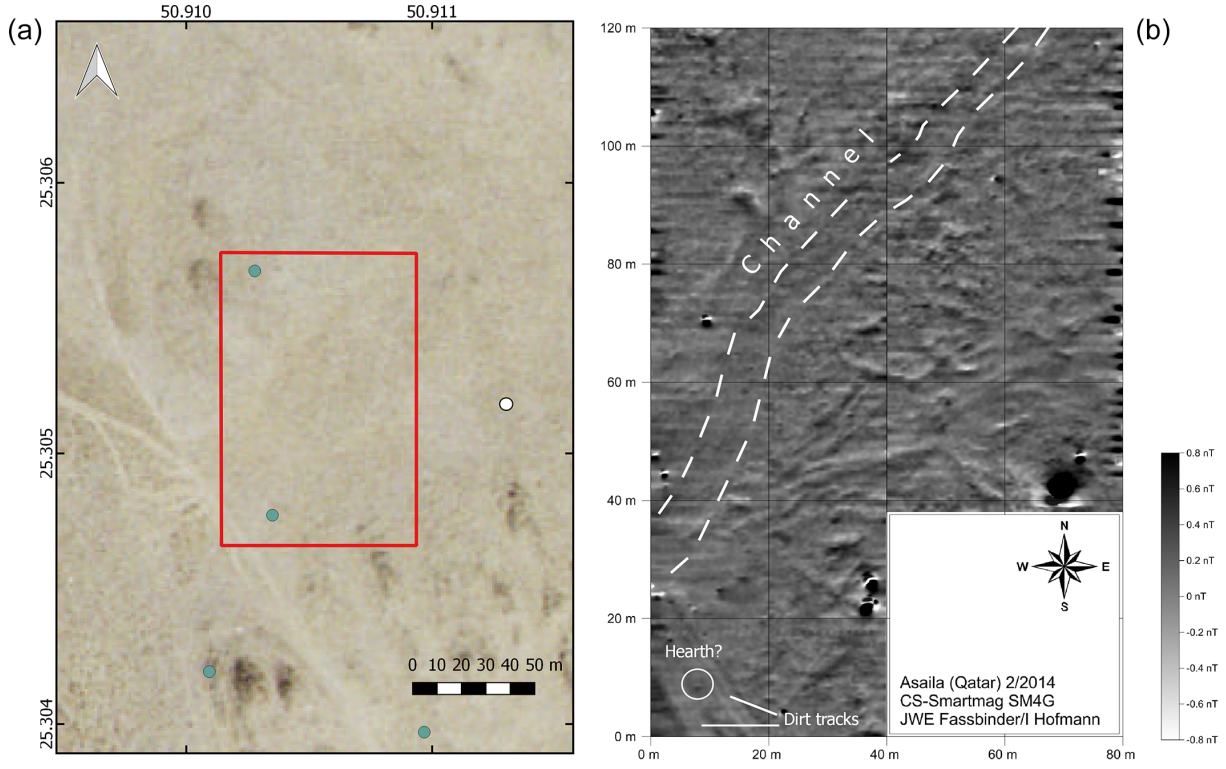

Figure 4. Magnetometer prospection (**b** and red frame in **a**) in the area of the Acila 36 excavation by Inizan (1988), located at the basinward end of the lower limestone plateau (see Fig. 1 for overview). The area, where several scatters of both worked and unworked flint (green dots on **a**) were found during the survey of Drechsler et al. (2016), some also associated with ceramics (white dot), slopes towards the southwest and merges into the sand and gravel sheets and the sabkha-type sand flats of the basin. The magnetogram shows an inactive, subsurface channel structure running towards the basin (white lines).

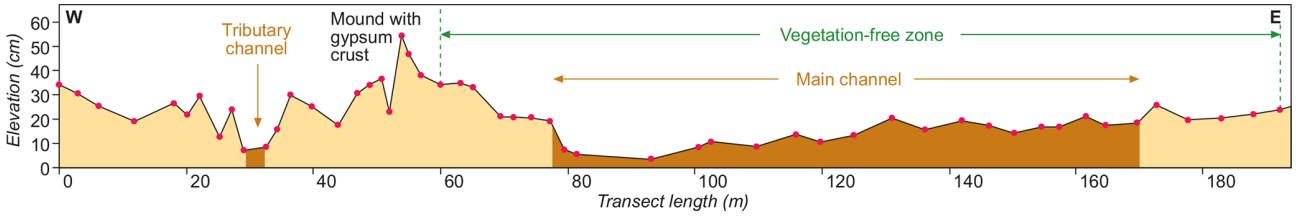

Figure 5. Elevation transect crossing the shallow and wide northern channel (green line in Fig. 2).

The amount of sand varies, while some sections (2.87–2.78, 1.53–1.33, 0.82–0.73 m b.s., uppermost 0.34 m) show a significant clay and silt component of up to 25 % (Fig. 7). The sand mostly consists of well-rounded quartz grains and minor appearances of feldspar, gypsum, reworked Dammam limestone and some dark heavy minerals. The sections with the highest amounts of silt and clay were checked for microfossil indicators for lacustrine environments, but only very isolated, highly abraded skeletal fragments were found. In most cases, the occasional gravel component coincides with large gypsum crystals, which occur in large numbers at several horizons, as either hardgrounds or gypsum mush (ca. 2.30, ca. 1.55, 1.00–0.90 m b.s., upper 20 cm). The sections 1.80–1.53 and 0.73–0.49 m b.s. appear well-stratified with alternating coarser and finer textures. Most sections are moderately sorted to moderately well-sorted, except those containing a more significant silt/clay or gypsum component.

4.4 The southern *riyad*

Two *riyad* were investigated (Fig. 8). At QAT 41 (site HAR 5183/QNHER 5183 in Gerber et al., 2013), a considerable surface relief has formed through wind sculpturing. The loose coarse sand on top is distributed in patches, partly developing wind ripples (Fig. 9b). While smaller limestone pebbles at the surface may result from sheet flood input into the endorheic depression of ca. 0.065 km^2, the small boulders, mostly found along the *rawdha* margins, were brought

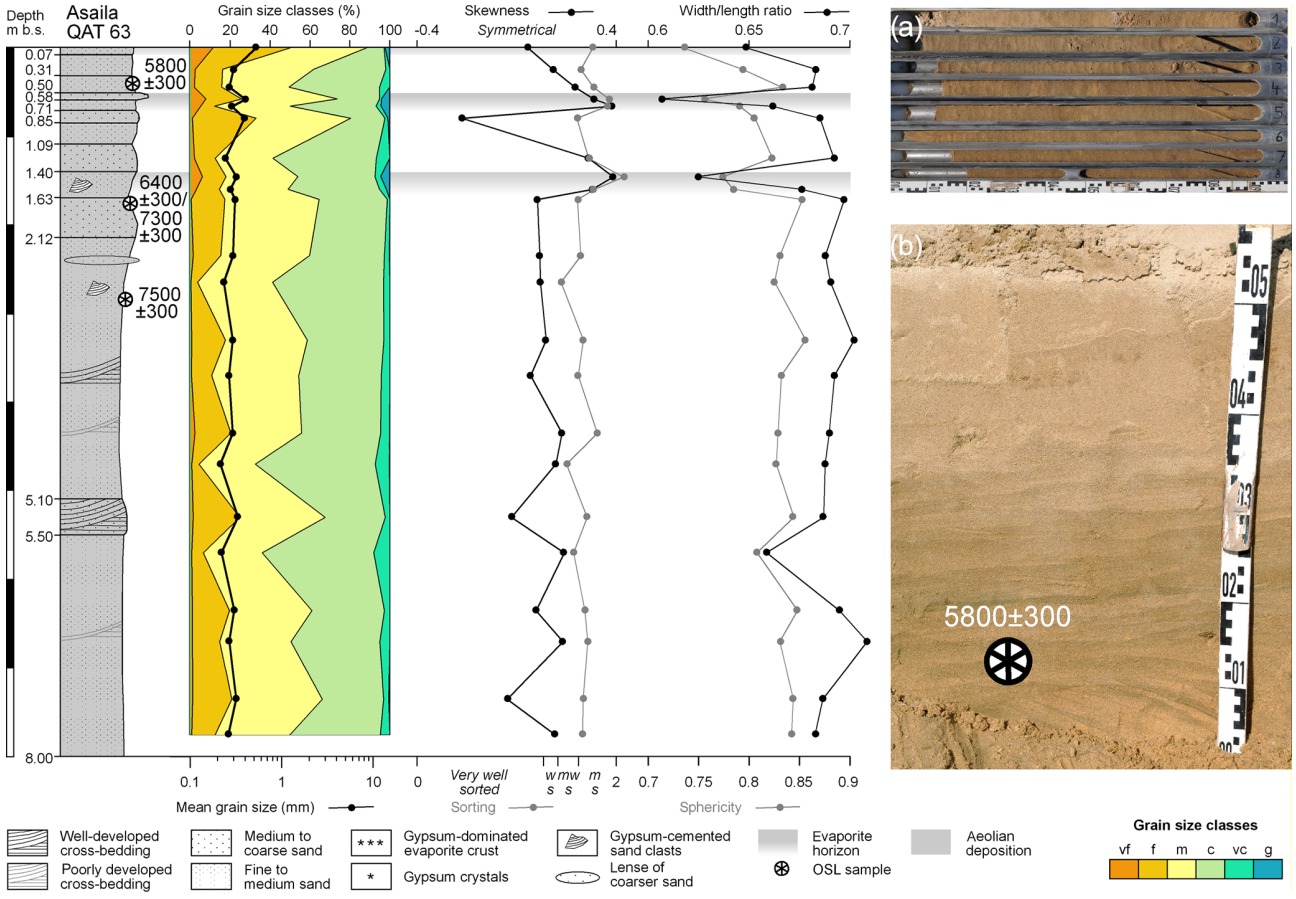

Figure 6. Vibracore QAT 63 from the lowest-lying sabkha-type sand flats of the western Asaila depression (see Fig. 1), showing core log, mean grain size, grain size classes (vf: very fine sand; f: fine sand; m: medium sand; c: coarse sand; vc: very coarse sand; g: gravel), sorting (ws: well-sorted; mws: moderately well-sorted; ms: moderately sorted), skewness, and the width to length ratio and sphericity of the grains (b.s.: below surface). **(a)** The entire core down to a depth of 8 m; **(b)** a close-up of the upper 50 cm of the stratigraphy with the position of the uppermost OSL sample and typical aeolian cross-bedding features (modified after Drechsler et al., 2016).

in by humans to stabilize their tents. Further archaeological findings comprise food remains (shells) (Gerber et al., 2014). A pit dug in the central part revealed only 80 cm of sedimentary infill. Overlying the Dammam limestone is a thin unconsolidated layer of limestone pebbles, up to 3 cm in diameter, in a fine sandy matrix. The section 0.75–0.48 m b.s. shows consolidated, greyish brown medium sand with a minor silt fraction as well as fine to coarse sand (Fig. 10). Furthermore, $CaCO_3$ concretions as pseudomorphs along former root channels were documented. The following layer (0.48–0.42 m b.s.) has a similar sand matrix but contains a greater amount of precipitated $CaCO_3$. The upper unit (0.42–0.00 m b.s.) consists of weakly consolidated silty fine sand with some carbonate concretions and root remains (Fig. 9b).

The two thicker units below and above the $CaCO_3$ horizon reveal OSL dates of 1200 ± 100 (0.60 m b.s.) and 710 ± 30 (0.30 m b.s.) years, respectively (Table S1). Since scatter and shape of equivalent dose distributions suggest relatively complete signal resetting prior to deposition (Fig. S4) and both samples are situated clearly above the groundwater level, the OSL ages provide robust estimates of the time of sediment deposition. Vertical sediment mixing through haloturbation potentially biasing the equivalent dose distributions can be excluded due to negligible salt contents (Babikir, 1986).

Sediment core QAT 66 was taken at the centre of a second, much larger *rawdha* (ca. 0.74 km^2) with a complex system of wadis entering from all sides (Fig. 8). QAT 66 hit bedrock at 0.79 m b.s., exposing an overlying sequence of consolidated, well-sorted, greyish light brown silt with a very small fine-sand component. Downcore changes are negligible. The deposit is compact and entirely dry. It forms an even surface with very sparse and low herbaceous vegetation grazed by goats and sheep. Shrubs trap aeolian sand and form nebkha mounds of > 1 m in elevation (Fig. 9a).

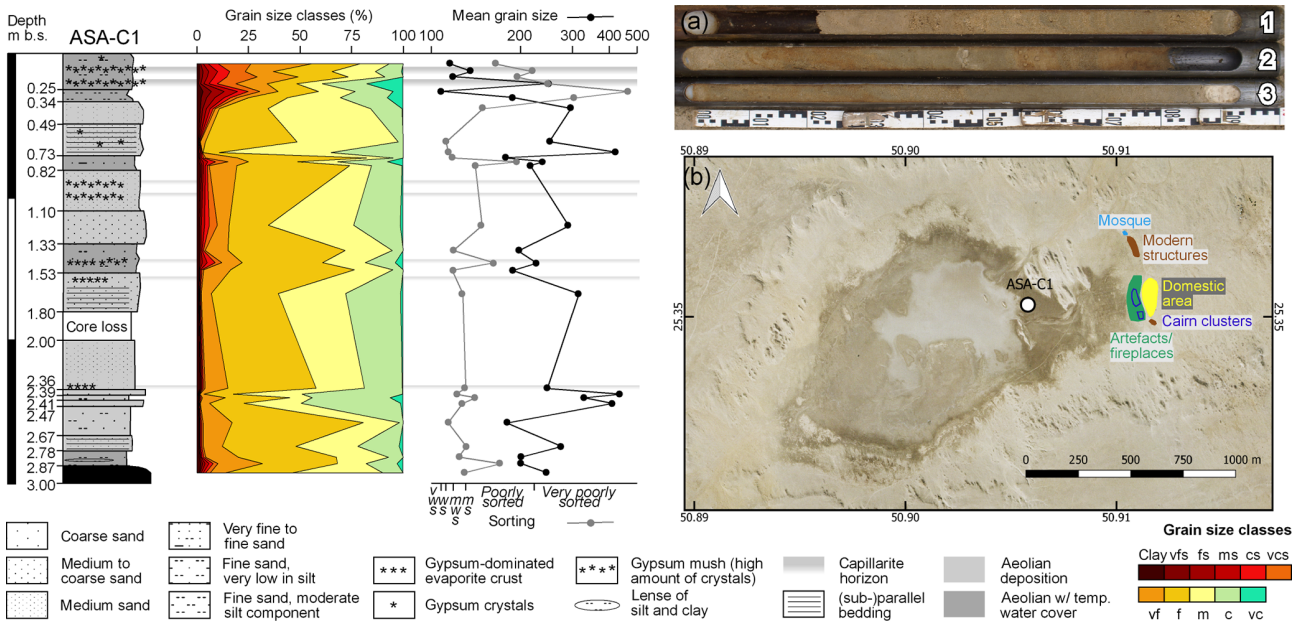

Figure 7. Vibracore ASA-C1 from the large-scale topographical depression of Jaow Aqeeq (Fig. 1), where limestone bedrock was encountered at 2.87 cm b.s. (below surface). Core log, mean grain size, grain size classes (vfs: very fine silt; fs: fine silt; mes: medium silt; cs: coarse silt; vcs: very coarse silt; vf: very fine sand; f: fine sand; m: medium sand; c: coarse sand; vc: very coarse sand) and sorting (vws: very well-sorted; ws: well-sorted; mws: moderately well-sorted; ms: moderately sorted) are shown. **(a)** The entire core down to a depth of 3 m. **(b)** Overview map of Jaow Aqeeq with coring site (basemap is IKONOS image of 2004) and archaeological surface findings according to Schönicke et al. (2016).

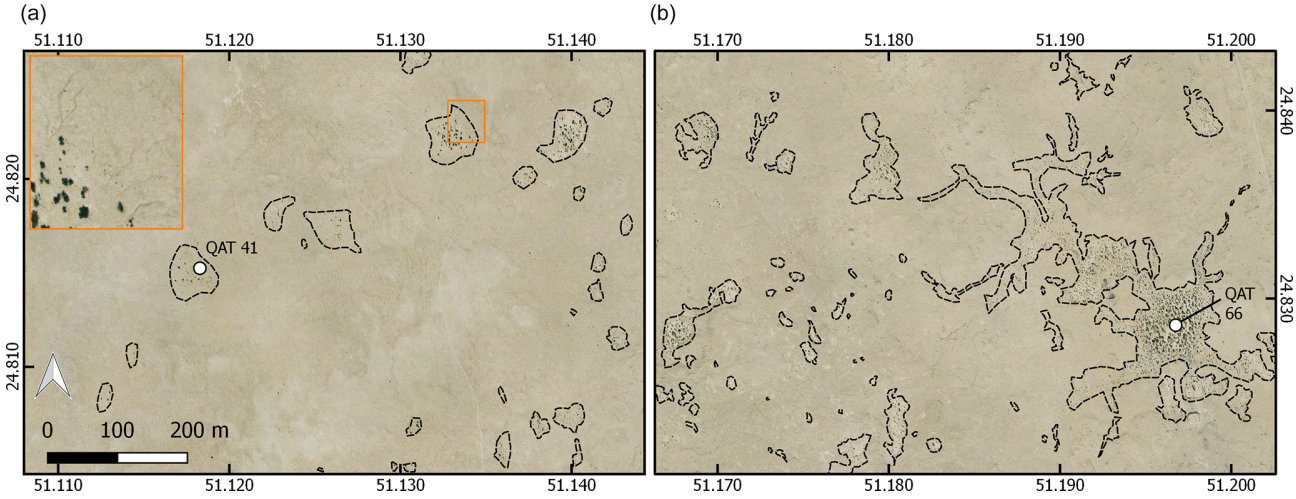

Figure 8. Map of *riyad* in south Qatar (see location in Fig. 1), which were investigated for their sediment infill during the SQSP (based on an IKONOS satellite image of 2004). The outlines of the *riyad* are mostly reflected by vegetation and, where they are more mature as in **(b)**, may develop extended networks of micro-wadis. Note the example of traces of surface discharge into the *riyad* in **(a)** (orange rectangle). QAT 41 represents a trench in *rawdha* HAR 5183 (Gerber et al., 2013) and QAT 66 a sediment core in a *rawdha*, which was not part of the archaeological survey (Fig. 9).

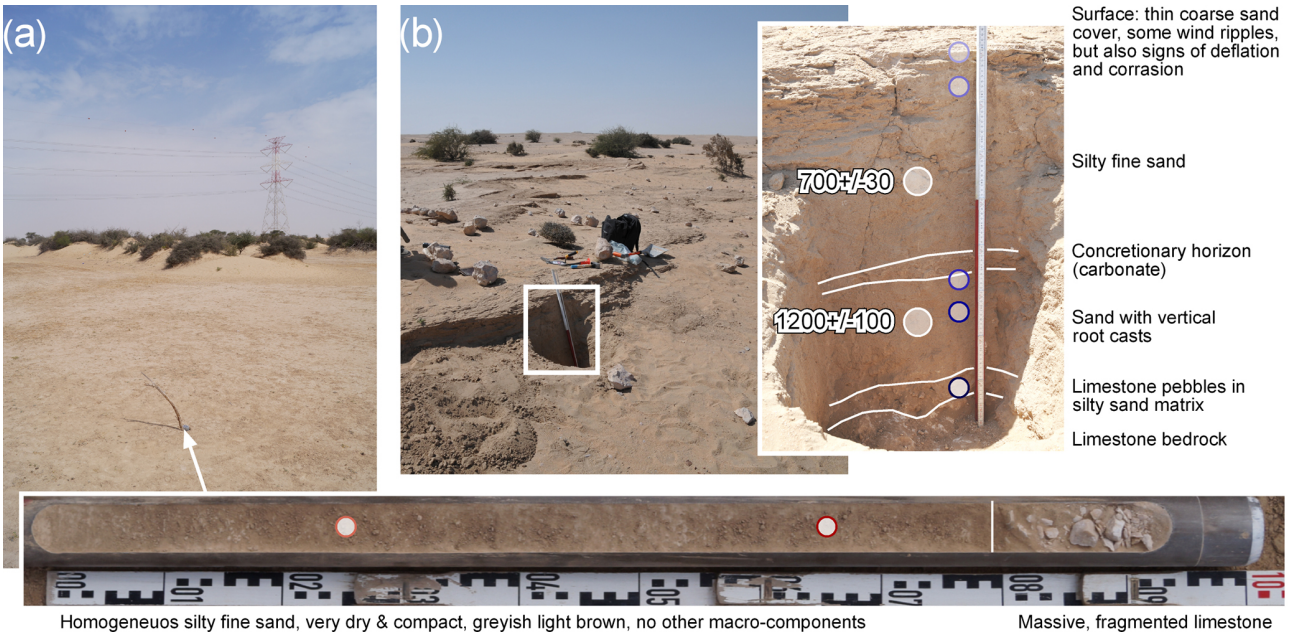

Figure 9. **(a)** Sediment core QAT 66 inside a larger *rawdha* with multiple wadis entering from all sides (Figs. 1, 8); the location of grain size samples is indicated on the core (Fig. 10). **(b)** Profile QAT 41 exposing the sediment infill of a smaller, more elliptic *rawdha* (HAR 5183), with brief stratigraphic log, OSL ages (Table S1) and grain size samples (Fig. 10).

5 Discussion

5.1 Holocene landscape dynamics of the Asaila basin

5.1.1 The geomorphic system

Geomorphic mapping based on field surveys and satellite imagery reveals the polygenetic nature of landforms in the Asaila basin, driven by tectonic, aeolian and fluvial processes as well as subsurface hydrology. The macroscale relief is determined by the roughly N–S-trending anticline or syncline structures, in particular the Al Huriyeh syncline (Fig. 1). The basin's origin may be controlled by a NNE–SSW-striking fault (Inizan, 1988) initiating long-term, subsurface limestone dissolution and collapse since the Miocene (Sadiq and Nasir, 2002) and eventually creating a large-scale morphological depression at the surface. Definite field evidence for such a fault, however, is missing, and other sources emphasize the lack of surface expressions of major faulting on the Qatar peninsula (e.g. Cavalier, 1970; Sadiq and Nasir, 2002).

Surface water exists but is very short-lived and only occurs episodically during strong rainfall. Geomorphic evidence was mapped in the eastern part, in the form of fluvial bedforms in a narrow, shallow channel and a collapsed (sub)surface drainage system, i.e. a potential karst spring. The wadi channel mapped in the central northern part of the basin with its reddish-brown surface appears inactive; halite as a potential sign of recent flooding is absent (sample ASA 7). However, it unequivocally represents a significant pathway of surface runoff into the basin. Another major pathway of surface inflow exists in the northernmost part of the basin, where the higher limestone plateau is dissected in an ENE–WSW orientation (Fig. 2). The small valley entering at the northernmost extension of the basin hosts a subsurface channel morphology (Fig. 4), testifying to the relict nature of more significant surface runoff. There is, however, no evidence for the timing of this increased runoff.

5.1.2 Prevalence of aeolian processes

Grain size measures of sediment core QAT 63 reflect a persisting aeolian environment. OSL data indicate that the sequence captures at least the entire Holocene. Both datasets in combination with present-day sabkha-type surfaces, nebkha formation, sand ripples, streamlined gypsum mounds showing clear signs of corrasion and sand ramps reflecting the main Shamal corridor show that aeolian processes have dominated the Asaila landscape at least since the arrival of humans in the Neolithic. QAT 63 rejects any type of lacustrine environment inside the Asaila basin during that time, which has been speculated by Macumber (2012).

5.1.3 Fluctuations of the groundwater table and capillary evaporite formation

The three horizons of poorly sorted sediments, as well as a lower width to length ratio and sphericity of grains in the uppermost 1.5 m of QAT 63 are related to the ongoing precipitation of mostly gypsum crystals from ascending groundwater in the vadose zone. These processes are similar to

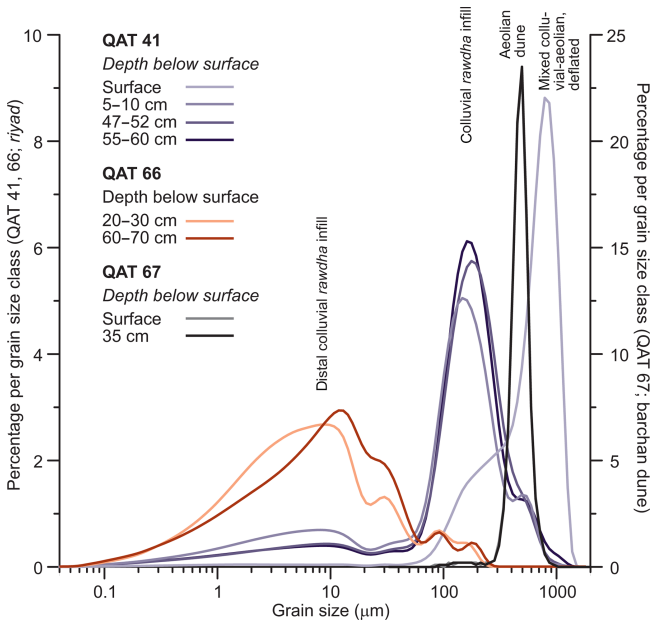

Figure 10. Grain size distribution of samples from the *riyad* (Fig. 9) and, for comparison, a typical barchan dune of south Qatar (QAT 67; curves almost entirely overlap).

those in continental sabkhas, where brines are significantly more highly concentrated (Sonnenfeld and Perthuisot, 1989; Yechieli and Wood, 2002; Ginau et al., 2012). Upward capillary movement from a shallow groundwater table (ca. 1.5 m deep in the Asaila basin today) leads to a halite-dominated and carbonate-containing crust at the surface, underlain by one or several layers of gypsum, also referred to as capillarites (Sonnenfeld and Perthuisot, 1989). This is also reflected by surface XRD samples from the hummocky sand flats, which, similar to the sabkha-type sand flats, represent active equilibrium surfaces of deflation and aeolian deposition. Crust formation is to a large extent driven by capillary rise and the position of the groundwater table. Sample ASA 3 still contains halite, whereas samples ASA 1 and 2 do not contain halite and show how easily salts are deflated and dissolved at the surface (Sonnenfeld and Perthuisot, 1989).

Even though Asaila is located at the southwestern fringe of the freshwater lens of Qatar (Fig. 1), subsurface gypsum dissolution in the Rus and underlying Umm er Radhuma Formations results in elevated levels of salinity and brackish to saline groundwater in the southern peninsula (Lloyd et al., 1987; Macumber, 2011, 2015). Asaila has relatively moderate salinity levels of around 3000 ppm (Macumber, 2012), which is still sufficient to precipitate capillary evaporites in the vadose zone and, in the eastern sabkha-type sand flats, thin buckled gypsum crusts at the surface. However, comparison with the sediment infill and the thick, halite-dominated surface crust at Jaow Aqeeq (ASA-C1) shows how a higher groundwater table and significantly higher groundwater salinity of about 8000 ppm (Macumber, 2012) may lead to more intense precipitation of evaporites in interstitial pore waters and the establishment of inland sabkha conditions. While Jaow Aqeeq seems to directly correspond with the Dukhan coastal sabkha in terms of hydrogeological exchange, the higher limestone plateau separating the Asaila depression from the southeasternmost extension of the Dukhan sabkha is also reflected by the strong SE–NW gradient on the groundwater salinity map in Macumber (2012).

5.1.4 The role of relative sea-level changes in landscape formation

The rate of aeolian sand sedimentation of 1–2 mm yr^{-1} in the upper 3 m of QAT 63 averaged over the time between ca. 7500 and 5800 years ago as inferred from OSL data is driven by two factors: (i) greater sand availability further north (upwind), as large parts of the Qatar peninsula were then still covered by dune fields (Engel et al., 2018), and, (ii) at that time, relative sea level, which is coupled with groundwater levels in low-lying areas near the Qatari coast (Macumber, 2011), rose by several metres (Lambeck, 1996), reaching a highstand around 6000 years ago (Perthuisot, 1977; Engel and Brückner, 2014; Parker et al., 2018; Strohmenger and Jameson, 2018; Rivers et al., 2020). A rising groundwater table and capillary fringe stabilize newly deposited sand in dry climates and lead to net accumulation. Such a raised equilibrium surface close to the shallow groundwater table is referred to as the Stokes surface, below which deflation does not occur due to cohesion of the sediment provided by capillary moisture and initial cementation (Fryberger et al., 1988). It seems that after the sea-level highstand phase (+2–3 m, ca. 6000–4500 years ago; Vita-Finzi, 1978; Cuttler and Al-Naimi, 2013; Engel and Brückner, 2014; Parker et al., 2018; Strohmenger and Jameson, 2018; Rivers et al., 2020), deflation began due to the lowering of the groundwater and the capillary fringe along with sea level, thereby affecting the lowering Stokes surface.

The characteristic mounds covering specific areas of the Asaila basin (Figs. 2, 3a) are mainly preserved by porous, platy or needle-shaped gypsum (surface samples ASA 5, 6, 8–10). We assume that these gypcretes are relict horizons of interstitial gypsum in the vadose zone at the time of the sea-level and groundwater-level highstand. Predominant deflation afterwards in the era of sinking groundwater levels led to the removal of the halite–carbonate surface crust (see Sonnenfeld and Perthuisot, 1989), the aeolian sand below and parts of the more massive gypsum crusts. Where the gypsum withstood erosion, the crust protected the underlying deposits from denudation resulting in the formation of mounds.

5.1.5 Origin of the linear mounds

The origin of the linear mounds (Figs. 2, 3b) in the central southern part of the basin, some of which form irregular grids, remains enigmatic. In some parts, they resemble

inverted canals as known from other arid environments, e.g. historical Lower Mesopotamia (Brückner, 2013; Engel and Brückner, 2018) or southern Peru (Beresford-Jones et al., 2009), but no other indication of an anthropogenic origin was found. Alternatively, the network of linear mounds could follow the pattern of subsurface small-scale joints, which provide better conditions for the capillary rise of water to form stable gypsum crusts. Further in-depth investigations are necessary to shed light on the origin of the linear shapes.

5.2 Landscape dynamics and the archaeological record

The limited availability of potable water has always determined ancient settlement patterns in Qatar, explaining why most archaeological sites are located on the northern peninsula. The generally poor groundwater quality in the southern part (Cuttler and Al-Naimi, 2013; Macumber, 2015) meant that Neolithic occupation concentrated mostly around the Asaila basin, where access is fairly easy and the salinity is moderate (Drechsler et al., 2016). Only in recent times have further potentially Palaeolithic and Neolithic sites been discovered closer to the coast (Drechsler, 2014). Several Early Neolithic flint knapping workshops were identified along the margins of the Asaila basin based on the spectrum of single diagnostic Qatar-B artefacts or artefact scatters (dated to ca. 7500–6500 BCE). They existed mostly in direct proximity to outcrops of flint raw material (Pfeiffer, 2015; Drechsler et al., 2016), comprising regular blades from bidirectional naviform cores (Inizan, 1988; Pelegrin and Inizan, 2013). In contrast, Middle Neolithic artefacts, i.e. unifacial and bifacial points, scrapers, and bifacially chipped winged and tanged arrowheads following the "Arabian bifacial lithic tradition" sensu Edens (1982, 1988) (ca. 6500–4500 BCE), show the greatest concentrations inside the basin (Fig. 11). They occur either as scatters of cores, flakes and flint tools in combination with burnt limestone and ashy sediment in the centre of the basin, indicating both in situ flint knapping and domestic activities, or as single tool findings at the lower western margins, where they point to incidental tool usage and discard (Drechsler et al., 2016). Successful refitting of single pieces of the same flint artefacts within a radius of only a few metres inside one of the survey units inside the basin shows that relocation of artefacts is negligible (Schönicke et al., 2016). There appears to have been quite a substantial occupation in the Middle Neolithic with a focus in the centre of the basin, which, at that time, might have provided a higher potential for grazing of both domesticated and wild animals (Drechsler et al., 2016).

Even though no local proxy record of Holocene climatic changes exists in Qatar, the high-resolution $\delta^{18}O$ curve from a speleothem at Hoti Cave, Oman (Fleitmann et al., 2007; Fig. 12b), and the palaeo-lacustrine record from Awafi near Ras al-Khaimah, UAE (Parker et al., 2016; Fig. 12d), may provide important references. Both sites received a moisture surplus during Early Holocene to mid-Holocene summer seasons from the Indian Summer Monsoon (Fleitmann et al., 2007) and even more so from the intensified East African Summer Monsoon (EASM) penetrating into the Arabian Peninsula. The role of the mid-level westerlies for the Early Holocene Humid Period (EHHP) in the southeastern Arabian Peninsula, however, remains unclear (Parker et al., 2016). Recent climate model simulations by Jennings et al. (2015) and Guagnin et al. (2016) suggest that Qatar might have had an increase in rainfall following an intensification of the African–Asian monsoonal systems, although far less than the sites of Awafi, Hoti Cave, or another site in south Oman, i.e. Qunf Cave (Fig. 12c). The onset of lacustrine conditions as reflected by the Ti and magnetic susceptibility records from Awafi (Parker et al., 2016; Fig. 12d) overlaps well with the intensification of Middle Neolithic occupation at Asaila (Drechsler et al., 2016; Fig. 12g), which at its later stage also benefitted from the high groundwater table connected to the sea-level highstand (Lambeck, 1996; Parker et al., 2018; Strohmenger and Jameson, 2018; Fig. 12e). The Hoti Cave record indicates an even earlier onset of the EHHP, which may reflect more favourable environmental conditions and incipient human occupation at Asaila already in the Early Neolithic (Fig. 12b, g). The same applies to the northern Arabian palaeolake record from Tayma (Saudi Arabia), which reflects only a very short EHHP and appears offset, probably due to a complex interplay of a range of global and regional atmospheric moisture sources, e.g. the EASM, Mediterranean winter rains and winter–spring tropical plumes (Engel et al., 2012; Enzel et al., 2015; Neugebauer et al., 2018; Parton et al., 2018).

Macumber (2018) associates the phase of a wetter climate around the 6th and 5th millennia BCE with the formation of a massive subterraneous freshwater lens over large parts of Qatar. The subsequent absence of archaeological traces at Asaila – and a reduction of sites in the entire country (Muhesen and Al-Naimi, 2014) as well as across the wider gulf region (Uerpmann, 2003) – is associated with aridification on the eastern and southeastern Arabian Peninsula, sea-level drop and associated groundwater level fall (at least after the highstand plateau ended around 2500 BCE), and the onset of a predominant deflation regime inside the basin. After a hiatus, Islamic (610–1972 CE) to Modern (post 1972 CE) pottery and remains of campsites were found (Figs. 11, 12g), along with cairns on the higher plateau (Gerber et al., 2014; Drechsler et al., 2016), which are difficult to date (Cuttler et al., 2013; Izquierdo Zamora et al., 2015).

5.3 *Rawdha* formation

The uniform sedimentary infill of south Qatar's shallow karst depressions (*riyad*) appears rather young. The one which was dated in this study (QAT 41) has accumulated its silts and sands over the last 2000–1500 years as determined by OSL data. The low ages of the sediment infill explain the absence of older archaeological findings, which, in the *riyad* surveyed

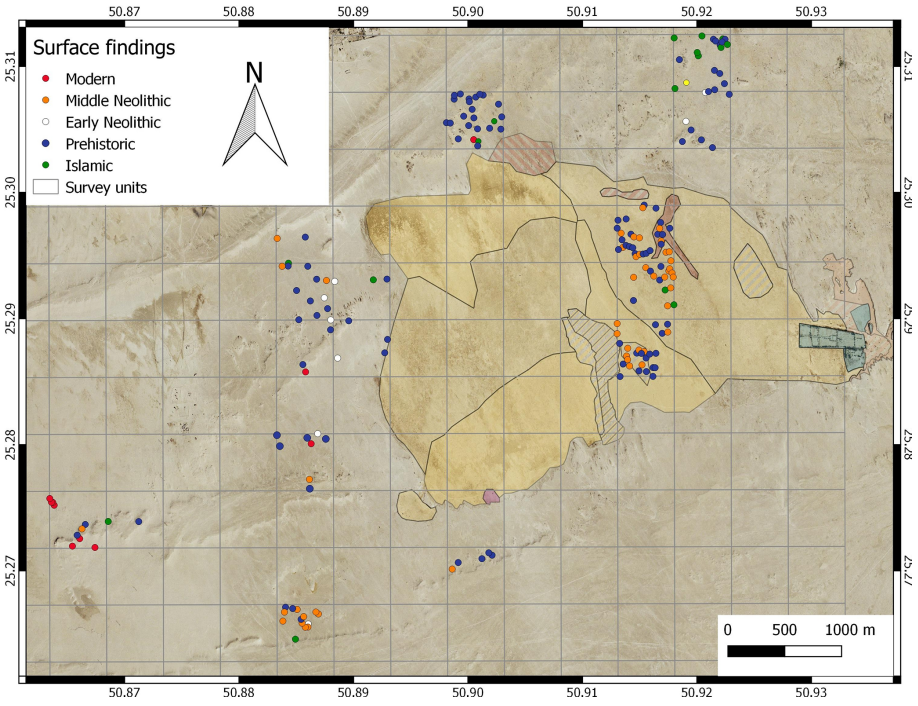

Figure 11. Spatial distribution of archaeological surface findings (basemap from IKONOS 2004) inside and around the Asaila basin. Selected squares (indicated by mapped surface findings) of 500 m × 500 m were surveyed by systematic back-and-forth walking in order to guarantee a 100 % coverage (Drechsler et al., 2016). Geomorphic units of the innermost Asaila basin are shown for orientation (see details in Fig. 2). "Prehistoric" refers to flint artefacts with unspecific character, which, in theory, may date from any period between the Palaeolithic and historical times (Drechsler et al., 2016).

by the SQSP, mainly consist of Late Islamic to Modern period pottery wares, modern trash, Chinese porcelain, coins or temporary mosque structures, all dating to the 18th century CE or younger (Eichmann et al., 2014; Schönicke et al., 2016).

Sedimentation inside the *riyad* is induced by surface runoff events as indicated by small wadi channels and runnels directed towards some of the larger landforms (Macumber, 2015; Fig. 8). The broad grain size distribution, in particular from the distal record inside the large *rawdha* (QAT 66), relates to colluvial processes, even though a contribution of aeolian dust as indicated by geochemical data from *riyad* surfaces of Qatar's interior presented by Yigiterhan et al. (2018) cannot be excluded. As small, endorheic basins, the *riyad* represent pivotal sites of meteoric groundwater recharge (Macumber, 2011, 2015; Cuttler and Naimi, 2013) and groundwater access through wells. They become flooded during rainfall events, which explains the distribution of remains of temporary camps only along their margins (Gerber et al., 2014; Schönicke et al., 2016). Accordingly, the silt component of their infill (Figs. 9, 10) settled out of suspension. Increased soil moisture, strong evaporation and significant sediment contributions of the local limestone-dominated hamada lead to carbonate crust formation in the vadose zone, as observed in QAT 41, and to incipient cementation. The finer grain size spectrum of QAT 66 (Fig. 10) compared to QAT 41 corresponds with its distal location in the centre of a very large *rawdha*.

Thus, net accumulation inside the *riyad* may represent a proxy for surface runoff, which is controlled by rainfall events and, as in our case, by land cover. In the Early Holocene and mid-Holocene, much of Qatar – most probably including the southern *riyad* – was covered and filled by mobile sands. Only after the southeastward migrating barchan dunes, which lost their source due to the transgression of the gulf (Embabi and Ashour, 1993; Engel et al., 2018), had left the *riyad* zone, could fine-grained colluvial deposits accumulate during surface runoff events. The *rawdha* HAR 5183 (QAT 41) is located ca. 21 km upwind of the migrating end of the barchan dunes west of Qatar's inland sea (Khor al-Udaid) (Fig. 1) according to the mean Shamal azimuth of 332° deviation from the north (Embabi and Ashour, 1993). This azimuth seems to have remained stable during the Holocene based on the similar orientation of drowned barchanoid dunes inside the Gulf of Salwa (Al-Hinai et al., 1987). Considering a migration rate of ca. 8–10 m yr^{-1} measured for medium-sized barchan dunes in Qatar over the time span of several decades (Engel et al., 2018), the karst depression became dune-free around ca. 2600–2100 years ago, or even later, if higher migration rates of smaller-sized barchan

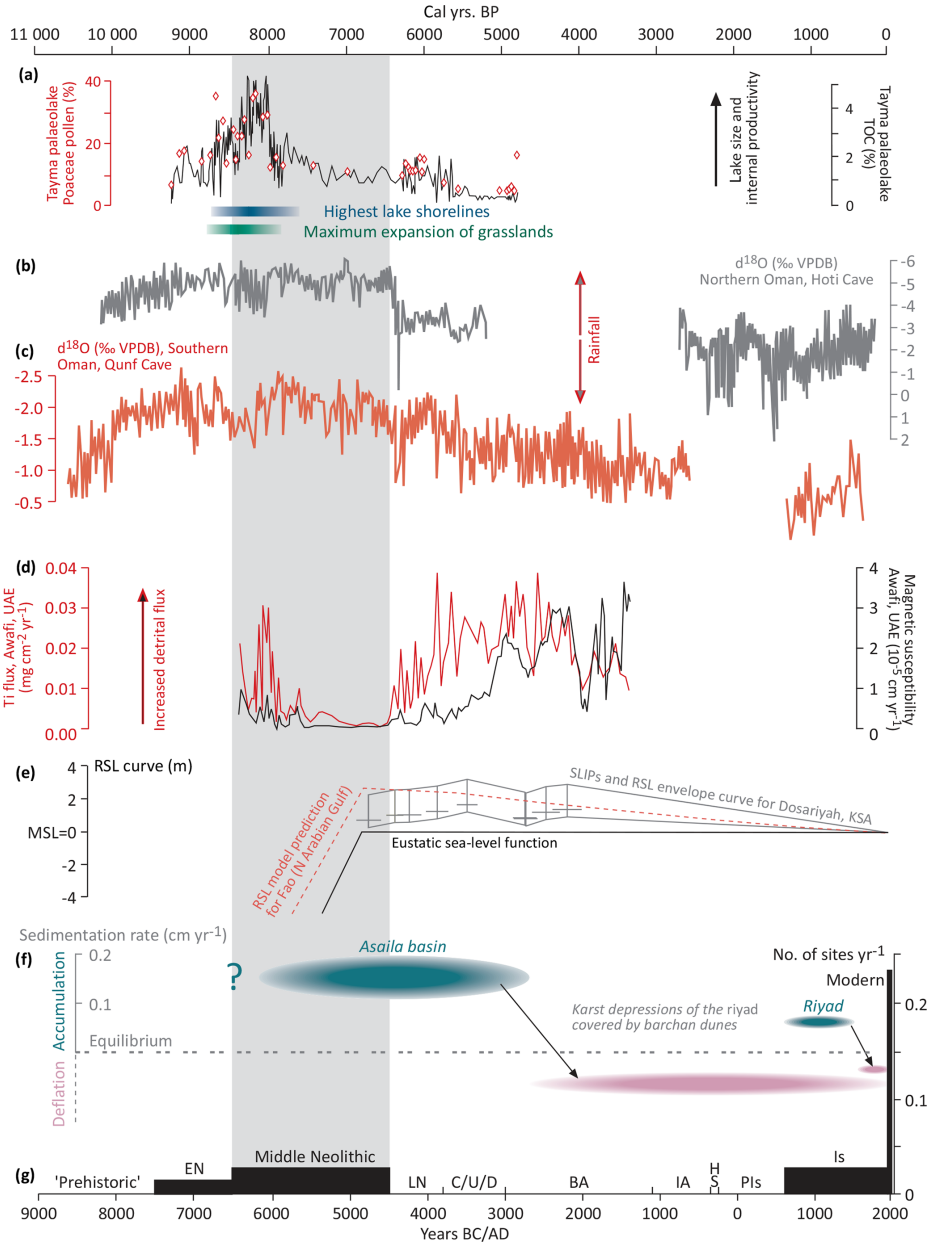

Figure 12. Synopsis of regional palaeoclimate and sea-level data in combination with accumulation–deflation phases in Asaila and the southern *riyad* as well as the chronological density of surface archaeological findings in Asaila. **(a)** TOC (total organic carbon) record and relative abundance of Poaceae pollen (grasses) (Dinies et al., 2016) combined with phases of the highest lake shorelines (Engel et al., 2012, considering revised chronology in Dinies et al., 2015) and maximum grassland expansion (Dinies et al., 2015) from the palaeo-lake and wetlands in the sabkha of Tayma, northern Arabia. Oxygen isotope records of stalagmites from **(b)** Hoti Cave, northern Oman, and **(c)** Qunf Cave, southern Oman (Fleitmann et al., 2007) (VPDB is relative to the Vienna Pee Dee Belemnite standard). **(d)** Ti flux and magnetic susceptibility from the lacustrine record of Awafi, UAE, where low values indicate landscape (dune) stability and higher moisture availability (Parker et al., 2016). **(e)** Envelope curve of relative sea-level stands from Dosariyah, Saudi Arabia, based on ^{14}C-dated sea-level index points considering vertical and lateral error margins (Parker et al., 2018). It is shown in combination with the global eustatic sea-level function and a regional modelled sea-level prediction for the northern head of the Arabian Gulf (Lambeck, 1996), the peak of which is tentatively shifted to account for ^{14}C calibration (MSL is mean sea level). **(f)** Sedimentation rates at Asaila and the southern *riyad* as inferred from OSL data of this study (Figs. 6, 9b, Table S1), and the inferred shift to a deflation regime. Barchan dune cover at *rawdha* QAT 41 was estimated based on migration rates inferred by Engel et al. (2018). Furthermore, the number of sites identified in and around the Asaila basin per year of the time span of each period is shown for the different historical and prehistoric periods (EN: Early Neolithic; MN; Middle Neolithic; LN: Late Neolithic; C: Chalcolithic; U: Uruk; D: Dilmun; BA: Bronze Age; IA: Iron Age; H: Hellenistic; S: Seleucid; PIs: pre-Islamic; Is: Islamic) as a proxy of the intensity of human occupation (Drechsler et al., 2016). The grey vertical bar crossing all proxy data curves emphasizes the Middle Neolithic, which is prominently represented by artefacts inside the Asaila basin (Fig. 11).

dunes are taken into account. This coincides with the start of the runoff-related silt and sand accumulation of the *rawdha* at some point before 1500 years ago, as inferred from OSL data. The archaeological record indicates significant human usage of the *riyad* during the last 300 years, when their infill already resembled today's situation. The only potential climate signal deduced from the surveyed *riyad* so far may be a shift to more pronounced aridity in very recent times indicated by ubiquitous surface deflation patterns and small, decimetre-scale yardangs (Figs. S33, S34). This process may have supported a concentration of young archaeological findings at the surface. Taking these observations into account, it can be concluded that the further north a *rawdha* is located, the longer it has been dune-free, and more time may be represented by its silty sediment record.

6 Conclusions

Among the diverse arid landform units of south Qatar, the Asaila basin as well as the numerous *riyad* of the central peninsula reveal the richest archaeological record. The former has a density of 108 surface findings per square kilometre extrapolated from the three surveyed squares inside the basin (Fig. 11). In contrast to previous maps of the Asaila basin, which only differentiate between "sabkha" and "aeolian deposits" (Al-Yousef, 2003), we demonstrate greater geomorphic variability and additional signs of (relict) surface runoff. The areas of mounds of different shapes – for the first time systematically investigated in this study – are important indicators for groundwater (and, thus, sea level) control of accumulation and deflation inside the basin. While the 8 m long sediment core reveals a continuous dominance of aeolian sedimentation over the Early Holocene to mid-Holocene, the mounds, cemented by capillary evaporites originally grown in the vadose zone, are a clear sign of deflation after the mid-Holocene sea-level (and groundwater-level) highstand. Abundant archaeological evidence of Early and Middle Neolithic occupation – the latter with a clear focus inside the Asaila basin – indicate more favourable living conditions. Whether these imply denser vegetation and better access to groundwater and are linked to the EHHP inferred from other records on the southeastern Arabian Peninsula (e.g. Fleitmann et al., 2007; Preston et al., 2012; Parker et al., 2016) still awaits verification. The existence of more favourable conditions inside the Asaila basin is particularly evident when compared with the adjacent basin of Jaow Aqeeq, which shows how a higher groundwater table and higher groundwater salinity are reflected by higher amounts of capillary gypsum and thicker surface evaporite crusts.

In contrast, the sediment records of the *riyad* in southern Qatar are very shallow, younger (only ca. 1500 years in the case of QAT 41) and apparently controlled by surface runoff, deflation and the constantly diminishing barchan dune cover over the Middle and Late Holocene (see Engel et al., 2018). The young age of the infill explains the exclusive presence of young artefacts, mainly covering the Late Islamic to Modern periods. In combination with the indicators of current deflation, it may relate to a decrease in rainfall and surface runoff in recent decades to centuries. Whether this shift is related to inactivity and burying of runoff channels identified at the northern margin of the Asaila (Figs. 4, 5) is a matter of future investigations. It remains to be stated that the Late Quaternary environmental changes on the peninsula of Qatar are still largely unknown due to a lack of suitable geological archives. This report adds to the scarce information available, e.g. from Wadi Debayān (e.g. Tetlow et al., 2013), northeast Qatar, or the Ras Abrouq peninsula north of Dukhan, where archaeological layers were encountered down to a depth of 2.6 m (Smith, 1978; Vita-Finzi, 1978), even though chronological resolution and climatic significance still need to be improved. In the future, geophysical prospection of the *riyad* further north, e.g. using the combined approach of electrical resistivity tomography and seismic refraction tomography as applied for dolines on Crete by Siart et al. (2010), may help to locate thicker *rawdha* infill with more detailed palaeoenvironmental information through a higher-resolution age model in combination with the analysis of grain size distribution, micromorphology, phytoliths or even pollen spectra.

Data availability. OSL and XRD data are provided in the Supplement file. All grain-size-related data will be provided by the corresponding author upon request.

Supplement. The supplement related to this article is available online at: https://doi.org/10.5194/egqsj-68-215-2020-supplement.

Author contributions. The study was conceived by ME and HB. The archaeological survey was led by CG, PD, KP and RE. PD provided data on the spatial distribution of archaeological findings in Asaila. Geomorphic mapping was performed by SR, ME, and AP. ME, HB, KP, AP, DW and SR took sediment cores. ME, HB and KP logged and sampled the *rawdha* trenches. JWB conducted the magnetometer prospection and data processing. DB measured luminescence signals and calculated ages. SO conducted XRD measurements and interpreted XRD spectra. ME and DW carried out sedimentological analyses. ME wrote the paper. All authors read, commented on and approved the paper.

Competing interests. The authors declare that they have no conflict of interest.

Special issue statement. This article is part of the special issue "Geoarchaeology and past human–environment interactions". It is not associated with a conference.

Acknowledgements. We thank H.E. Shaykha al-Mayassa bint Hama bin Khalifah Al-Thani and H.E. Shaykh Hassan bin Muhammad Al-Thani without whose interest and support the joint South Qatar Survey Project of Qatar Museums (QM), represented by Faisal Abdulla Al-Naimi, Thomas Leisten, Alice Bianchi and Ferhan Sakal, and the German Archaeological Institute (DAI) (https://www.dainst.org/en/projekt/-/project-display/612902; last access 4 November 2019), would not have been realized. Nina Szemkus is acknowledged for supporting the laboratory work. Comments by the three anonymous reviewers and the handling editor Hans von Suchodoletz helped to significantly improve the paper.

Financial support. This research has been supported by Qatar Museums.

References

Al-Hinai, K. G., McMahon Moore, J., and Bush, P. R.: LANDSAT image enhancement study of possible submerged sand-dunes in the Arabian Gulf, Int. J. Remote Sens., 8, 251–258, https://doi.org/10.1080/01431168708948639, 1987.

Al-Naimi, F. A., Cuttler, R., Arrock, H., and Roberts, H.: A possible Upper Palaeolithic and Early Holocene flint scatter at Ra's 'Ushayriq, western Qatar, Proc. Sem. Arab. Stud., 40, 35–39, 2010.

Al-Naimi, F., Price, K. M., Cuttler, R., and Arrock, H.: Reassessing Wādī Debayan (Wādī al-abay'ān): an important Early Holocene Neolithic multi-occupational site in western Qatar, Proc. Sem. Arab. Stud., 41, 239–244, 2011.

Al-Saad, H.: Lithostratigraphy of the Middle Eocene Dammam Formation in Qatar, Arabian Gulf: Effects of sea-level fluctuations along a tidal environment, J. Asian Earth Sci., 25, 781–789, https://doi.org/10.1016/j.jseaes.2004.07.009, 2005.

Al Senafi, F. and Anis, A.: Shamals and climate variability in the Northern Arabian/Persian Gulf from 1973 to 2012, Int. J. Climatol., 35, 4509–4528, https://doi.org/10.1002/joc.4302, 2015.

Al-Yousef, M.: Mineralogy, Geochemistry and the origin of Quaternary sabkhas in the Qatar Peninsula, Arabian Gulf, PhD thesis, Faculty of Earth Sciences, University of Southampton, UK, 438 pp., 2003.

Babikir, A. A. A.: The vegetation of natural depressions in Qatar in relation to climate and soil, J. Arid Environ., 10, 165–173, https://doi.org/10.1016/S0140-1963(18)31236-9, 1986.

Batanouny, K. H.: Ecology and flora of Qatar, Alden Press, Oxford, 1981.

Benazzouz, M. T.: Hamada, in: Encyclopedia of Geomorphology, edited by: Goudie, A., Routledge, London, 512–513, 2004.

Beresford-Jones, D., Lewis, H., and Boreham, S.: Linking cultural and environmental change in Peruvian prehistory: Geomorphological survey of the Samaca Basin, Lower Ica Valley, Peru, Catena, 78, 234–249, https://doi.org/10.1016/j.catena.2008.12.010, 2009.

Bibby, G.: Arabian Archaeology, Kuml, 15, 133–152, 1965.

Billeaud, I., Caline, B., Livas, B., Tessier, B., Davaud, E., Frébourg, G., Hasler, C.-A., Laurier, D., and Pabian-Goyheneche, C.: The carbonate-evaporite lagoon of Al Dakhirah (Qatar): an example of a modern depositional model controlled by long-shore transport, Geol. Soc. London Spec. Pub., 388, 561–588, https://doi.org/10.1144/SP388.7, 2014.

Blott, S. J. and Pye, K.: GRADISTAT: a grain size distribution and statistics package for the analysis of unconsolidated sediments, Earth Surf. Proc. Land., 26, 1237–1248, https://doi.org/10.1002/esp.261, 2001.

Breeze, P. S., Groucutt, H. S., Drake, N. A., Louys, J., Scerri, E. M. L., Armitage, S. J., Zalmout, I. S. A., Memesh, A. M., Haptari, M. A., Soubhi, S. A., Matari, A.H., Zahir, M., Al-Omari, A., Alsharekh, A. M., and Petraglia, M. D.: Prehistory and palaeoenvironments of the western Nefud Desert, Saudi Arabia, Archaeol. Asia, 10, 1–16, https://doi.org/10.1016/j.ara.2017.02.002, 2017.

Brückner, H.: Wasserstraßen im Wüstensand, Antike Welt, 44, 18–24, 2013.

Buckley, D. G.: The excavation of seven cairns on the Ras Aburuk peninsula, in: Qatar Archaeological Report – Excavations 1973, edited by: De Cardi, B., Oxford University Press, Oxford, UK, 120–135, 1978.

Carter Jr., R. and Killick, R. (Eds.): Al-Khor Island: Investigating Coastal Exploitation in Bronze Age Qatar, Moonrise Press, Ludlow, UK, 2010.

Cavalier, C.: Geological description of the Qatar Peninsula (Arabian Gulf), Government of Qatar, Department of Petroleum Affaires, Doha, 1970.

Cuttler, R., Tetlow, E., and Al-Naimi, F.: Assessing the value of palaeoenvironmental data and geomorphological processes for understanding Late Quaternary population dynamics in Qatar, Proc. Sem. Arab. Stud., 41, 47–60, 2011.

Cuttler, R., Al-Naimi, F., and Tetlow, E.: Typological and chronological variation of burial in Qatar: 'Ubaid to late pre-Islamic, Proc. Sem. Arab. Stud., 43, 99–109, 2013.

Cuttler, R. T. and Al Naimi, F. A.: From land-locked desert to maritime nation: Landscape evolution and taphonomic Pathways in Qatar from 14 ka, Adumatu, 28, 7–22, 2013.

De Cardi, B. (Ed.): Qatar Archaeological Report, Excavations 1973, Oxford University Press, Oxford, UK, 1978.

Dinies, M., Plessen, B., Neef, R., and Kürschner, H.: When the desert was green: Grassland expansion during the early Holocene in northwestern Arabia, Quatern. Int., 382, 293–302, https://doi.org/10.1016/j.quaint.2015.03.007, 2015.

Dinies, M., Neef, R., Plessen, B., and Kürschner, H.: Holocene vegetation in northwestern Arabia – changing natural resources, in: Actualités des recherches archéologiques en Arabie, edited by: Goy, J., Bessenay-Prolonge, J., Betouche, A., Decaix, A., Havé, A., Hiblot, S., Perriot, C., and Pichon, F., Routes de l'Orient, Hors-Séries, 2, 1–19, 2016.

Drechsler, P.: The Palaeolithic and Neolithic in South Qatar, Insights from Two Seasons in the Field, Z. Orient Archäol., 7, 276–289, 2014.

Drechsler, P., Berthold, C., Al-Naimi, F. A., and Eichmann, R.: Ceremonial objects or household items? Non-destructive μ-XRD 2 and μ-XRF studies on three Neolithic hematite axes from Qatar, Arab. Archaeol. Epigr., 24, 119–124, https://doi.org/10.1111/aae.12029, 2013.

Drechsler, P., Engel, M., Brill, D., and Gerber, C.: The Asaila depression, an archaeological landscape in Qatar, Proc. Sem. Arab. Stud., 46, 98–106, 2016.

Edens, C.: Towards a definition of the western Rub al-Khali "Neolithic", Atlal, 6, 109–124, 1982.

Edens, C.: The Rub al-Khali "Neolithic" revisited: the view from Nadqan, in: Araby the Blest, edited by: Potts, D. T., CNI Publications, Copenhagen, 5–43, 1988.

Edens, C.: Khor Ile-Sud, Qatar: The archaeology of Late Bronze Age purple-dye production in the Arabian Gulf, Iraq, 61, 71–88, https://doi.org/10.2307/4200468, 1999.

Eichmann, R., Gerlach, I., Drechsler, P., Pfeiffer, K., and Gerber, C.: Joint Qatari-German project – Exploration and visualization of cultural heritage in south Qatar, World Herit., 72, 78–87, 2014.

Embabi, N. S. and Ashour, M. M.: Barchan dunes in Qatar, J. Arid Environ., 25, 49–69, https://doi.org/10.1006/jare.1993.1042, 1993.

Engel, M. and Brückner, H.: The South Qatar Survey Project (SQSP): Preliminary findings on Holocene coastal changes and geoarchaeological archives, Z. Orient Archäol., 7, 290–301, 2014.

Engel, M. and Brückner, H.: Holocene climate variability of Mesopotamia and its impact on the history of civilization, EarthArXiv, https://doi.org/10.31223/osf.io/s2aqt, 2018.

Engel, M., Brückner, H., Pint, A., Wellbrock, K., Ginau, A., Voss, P., Grottker, M., Klasen, N., and Frenzel, P.: The early Holocene humid period in NW Saudi Arabia – evidence from sediments, microfossils and palaeo-hydrological modelling, Quatern. Int., 266, 131–141, https://doi.org/10.1016/j.quaint.2011.04.028, 2012.

Engel, M., Matter, A., Parker, A. G., Parton, A., Petraglia, M. D., Preston, G. W., and Preusser, F.: Lakes or wetlands? A comment on "The middle Holocene climatic records from Arabia: Reassessing lacustrine environments, shift of ITCZ in Arabian Sea, and impacts of the southwest Indian and African monsoons" by Enzel et al., Global Planet. Change, 148, 258–267, https://doi.org/10.1016/j.gloplacha.2016.11.001, 2017.

Engel, M., Boesl, F., and Brückner, H.: Migration of barchan dunes in Qatar–controls of the Shamal, teleconnections, sea-level changes and human impact, Geosciences, 8, 240, https://doi.org/10.3390/geosciences8070240, 2018.

Enzel, Y., Kushnir, Y., and Quade, J.: The middle Holocene climatic records from Arabia: reassessing lacustrine environments, shift of ITCZ in Arabian Sea, and impacts of the southwest Indian and African monsoons, Global Planet. Change, 129, 69–91, https://doi.org/10.1016/j.gloplacha.2015.03.004, 2015.

Fassbinder, J. W. E.: Seeing beneath the farmland, steppe and desert soil: Magnetic prospecting and soil magnetism, J. Archaeol. Sci., 56, 85–95, https://doi.org/10.1016/j.jas.2015.02.023, 2015.

Fassbinder, J. W. E.: Magnetometry for Archaeology, in: Encyclopedia of Geoarchaeology, edited by: Gilbert, A. S., Springer, Dordrecht, 499–514, https://doi.org/10.1007/978-1-4020-4409-0_169, 2017.

Fleitmann, D., Burns, S. J., Mangini, A., Mudelsee, M., Kramers, J., Villa, I., Neff, U., Al-Subbary, A. A., Buettner, A., Hippler, D., and Matter, A.: Holocene ITCZ and Indian monsoon dynamics recorded in stalagmites from Oman and Yemen (Socotra), Quaternary Sci. Rev., 26, 170–188, https://doi.org/10.1016/j.quascirev.2006.04.012, 2007.

Fryberger, S. G., Schenk, C. J., and Krystinik, L. F.: Stokes surfaces and the effects of near-surface groundwater-table on aeolian deposition, Sedimentology, 35, 21–41, https://doi.org/10.1111/j.1365-3091.1988.tb00903.x, 1988.

Gerber, C., Drechsler, P., Yaşin-Meier, D., Brückner, H., Engel, M., Tiltmann, S., Atas, N., Bley, J., Daitche, J., Hörwarthner, D., Lienig, A., Reising, R., and Riesenberg, M.: The South Qatar Survey Project (SQSP) – Final Report of the 2013 Spring Season. Qatar Museums (Doha) & German Archaeological Institute (Berlin), 141 pp., 2013.

Gerber, C., Drechsler, P., Yasin-Meier, D., Brückner, H., Engel, M., Meier, D. M. P., Götzelt, T., Daitche, J., Hörwarthner, D., Lienig, A., Reising, R., and Tiltmann, S.: The German-Qatari South Qatar Survey Project: The 2012–2013 Season, Z. Orient Archäol., 7, 248–275, 2014.

Ginau, A., Engel, M., and Brückner, H.: Holocene chemical precipitates in the continental sabkha of Tayma (NW Saudi Arabia), J. Arid Environ., 84, 26–37, https://doi.org/10.1016/j.jaridenv.2012.03.020, 2012.

Glob, P. V.: Oldtidsfund i Qatar, Kuml, 7, 167–178, 1958.

Goudie, A. (Ed.): Nebkha, in: Encyclopedia of Geomorphology, Routledge, London, 708, 2004a.

Goudie, A. (Ed.): Stone pavement, in: Encyclopedia of Geomorphology, Routledge, London, 998–999, 2004b.

Guagnin, M., Jennings, R., Eager, H., Parton, A., Stimpson, C., Groucutt, H. S., Drake, N. A., Pfeiffer, M., Stepanek, C., Alsharekh, A., and Petraglia, M. D.: Rock art imagery as a proxy for Holocene environmental change: a view from Shuwaymis, NW Saudi Arabia, Holocene, 26, 1822–1834, https://doi.org/10.1177/0959683616645949, 2016.

Guérin, A. and Al-Naimi, F.: Territory and settlement patterns during the Abbasid period (ninth century AD): the village of Murwab (Qatar), Proc. Sem. Arab. Stud., 39, 181–196, 2009.

Heberger, M. and Donnelly, K.: Oil, Food, and Water: Challenges and Opportunities for California Agriculture, Technical Report, Pacific Institute, Oakland, 2015.

Inizan, M.-L. (Ed.): Préhistoire à Qatar. Mission archéologique française à Qatar (2), Éditions Recherche sur les Civilisations, Paris, France, 1988.

Izquierdo Zamora, Á., Cuttler, R. T. H., and Al-Naimi, F. A.: Prehistoric and pre-Islamic burial archaeology in Qatar: new results and perspectives, Proc. Sem. Arab. Stud., 45, 159–173, 2015.

Jennings, R. P., Singarayer, J., Stone, E. J., Krebs-Kanzow, U., Khon, V., Nisancioglu, K. H., Pfeiffer, M., Zhang, X., Parker, A., Parton, A., Groucutt, H. S., White, T. S., Drake, N. A., and Petraglia, M. D.: The greening of Arabia: multiple opportunities for human occupation of the Arabian Peninsula during the late Pleistocene inferred from an ensemble of climate model simulations, Quatern. Int., 382, 181–199, https://doi.org/10.1016/j.quaint.2015.01.006, 2015.

Kainert, C. and Drechsler, P.: An interplay of imports and local traditions? The pottery assemblage from Dosariyah, Saudi Arabia, Proc. Sem. Arab. Stud., 44, 213–226, 2014.

Kapel H.: Atlas of the Stone-Age Cultures of Qatar. Reports of the Danish Archaeological Expedition to the Arabian Gulf, Jutland Archaeol. Soc. Pub., 6, 5–43, 1967.

Konishi, M., Gotoh, T., and Akashi, Y.: Archaeological researches in the Gulf – A Preliminary Report of the Excavations in Bahrain and Qatar, 1987/8 Season, Orient, 24, 18–46, https://doi.org/10.5356/orient1960.24.18, 1988.

Lambeck, K.: Shoreline reconstructions for the Persian Gulf since the last glacial maximum, Earth Planet. Sc. Lett., 142, 43–57, https://doi.org/10.1016/0012-821X(96)00069-6, 1996.

Lloyd, J. W., Pike, J. G., Eccleston, B. L., and Chidley, T. R. E.: The hydrogeology of complex lens conditions in Qatar, J. Hydrol., 89, 239–258, https://doi.org/10.1016/0022-1694(87)90181-8, 1987.

Macumber, P. G.: A geomorphological and hydrological underpinning for archaeological research in northern Qatar, Proc. Sem. Arab. Stud., 41, 187–200, 2011.

Macumber, P. G.: An examination of the impact of environmental disparity on the occupation of Qatar – Season 4, Copenhagen University Study of the Archaeology of Qatar, unpublished report, 96 pp., 2012.

Macumber, P. G.: Water heritage in Qatar, in: Cultural Heritages of Water: Thematic Study on The Cultural Heritages of Water in the Middle East and Maghreb, edited by: UNESCO World Heritage Convention, UNESCO, 223–239, 2015.

Macumber, P. G.: Sea level and climatic influences on the occupation of Qatar and the Gulf during the Holocene period, Proc. Sem. Arab. Stud., 48, 201–217, 2018.

McPhillips, S., Rosendahl, S., and Morgan, V.: Abbasid rural settlement in northern Qatar: seasonal tribal exploitation of an arid environment?, Proc. Sem. Arab. Stud., 45, 185–197, 2015.

Muhesen, S. and Al-Naimi, F.: Archaeological heritage of pre-Islamic Qatar, World Herit., 72, 46–53, 2014.

Neugebauer, I., Dinies, M., Plessen, B., Dräger, N., Brauer, A., Frenzel, P., Gleixner, G., Hoelzmann, P., Krahn, K., Pint, A, Schwab, V.F., Schwarz, A., Tjallingii, R., and Engel, M.: The Early Holocene Humid Period in N Arabia – proxy evidence from a unique varved lake record, Geophys. Res. Abstr., 20, EGU2018-15815, 2018.

Norton, J., Abdul Majid, S., Allan, D., Al Safran, M., Böer, B, and Richer, R.: An Illustrated Checklist of the Flora of Qatar, Ashford Colour Press Ltd, Gosport, 2009.

Oates, J.: 'Ubaid Mesopotamia and its relation to Gulf countries, in: Qatar Archaeological Report – Excavations 1973, edited by: De Cardi, B., Oxford University Press, Oxford, 39–52, 1978.

Parker, A. G., Preston, G. W., Parton, A., Walkington, H., Jardine, P. E., Leng, M. J., and Hodson, M. J.: Low latitude Holocene hydroclimate derived from lake sediment flux and geochemistry, J. Quaternary Sci., 31, 296 –299, https://doi.org/10.1002/jqs.2859, 2016.

Parker, A. G., Armitage, S. J., Engel, M., Morley, M. W., Parton, A., Preston, G. W., and Russ, H.: Geomorphology, geoarchaeology and palaeoenvironments, in: Dosariyah – An Arabian Neolithic Coastal Community in the Central Gulf, edited by: Drechsler, P., Archaeopress, Oxford, UK, 21–55, 2018.

Parton, A., Clark-Balzan, L., Parker, A. G., Preston, G.W., Sung, W. W., Breeze, P. S., Leng, M. J., Groucutt, H. S., White, T. S., Alsharekh, A., and Petraglia, M. D.: Middle-late Quaternary palaeoclimate variability from lake and wetland deposits in the Nefud Desert, Northern Arabia, Quaternary Sci. Rev., 202, 78–97, https://doi.org/10.1016/j.quascirev.2018.10.010, 2018.

Pelegrin, J. and Inizan, M.-L.: Soft hammerstone percussion use in bidirectional blade-tool production at Acila 36 and in bifacial knapping at Shagra (Qatar), Arab. Archaeol. Epigr., 24, 79–86, https://doi.org/10.1111/aae.12016, 2013.

Perthuisot, J.-P.: Contribution à l'étude du Quaternaire marine de la péninsule de Qatar, Bull. Soc. Géol. France, S7-XIX, 1167–1170, https://doi.org/10.2113/gssgfbull.S7-XIX.5.1167, 1977.

Perthuisot, J.-P.: Le Quaternaire de la péninsule, données liminaires et hypothèses, in: Mission archéologique à Qatar, tome 1, edited by: Tixier, J., Doha, 11–31, 1980.

Pfeiffer, K.: South Qatar Survey Project, Katar: Archäologische Surveys in der südlichen Landeshälfte Katars, e-Forschungsber. DAI, 3, 79–82, 2015.

Preston, G. W., Parker, A. G., Walkington, H., Leng, M. J., and Hodson, M. J.: From nomadic herder-hunters to sedentary farmers: the relationship between climate change and ancient subsistence strategies in south-eastern Arabia, J. Arid Environ., 86, 122–130, https://doi.org/10.1016/j.jaridenv.2011.11.030, 2012.

Rao, P. G., Al-Sulaiti, M., and Al-Mulla, A. H.: Winter shamals in Qatar, Arabian Gulf, Weather, 56, 444–451, https://doi.org/10.1002/j.1477-8696.2001.tb06528.x, 2001.

Rees, G., Richter, T., and Walmsley, A.: Investigations in al-Zubārah hinterland at Murayr and al-Furayah, north-west Qatar, Proc. Sem. Arab. Stud., 41, 309–316, 2011.

Rivers, J., Engel, M., Dalrymple, R., Yousif, R., Strohmenger, C. J., and Al-Shaikh, I.: Are carbonate barrier islands mobile? Insights from a mid to late-Holocene system, Al Ruwais, northern Qatar, Sedimentology, 67, 534–558, https://doi.org/10.1111/sed.12653, 2020.

Sadiq, A. M. and Nasir, S. J.: Middle Pleistocene karst evolution in the State of Qatar, Arabian Gulf, J. Cave Karst Stud., 64, 132–139, 2002.

Schönicke, J., Tiltmann, S., Drechsler, P., Engel, M., and Pfeiffer, K.: South Qatar Survey Project (SQSP) Qatari-German Joint Archaeological Fieldwork by QM (Doha) and DAI (Berlin) – Final Report of the 2016 Spring Season, Qatar Museums (Doha) & German Archaeological Institute (Berlin), 103 pp., 2016.

Scott-Jackson, J. E., Rose, J. I., Scott-Jackson, W., and Al-Naimi, F.: Found: the Palaeolithic of Qatar, Proc. Sem. Arab. Stud., 45, 329–336, 2015.

Siart, C., Hecht, S., Holzhauer, I., Altherr, R., Meyer, H. P., Schukraft, G., Eitel, B., Bubenzer, O., and Panagiotopoulos, D.: Karst depressions as geoarchaeological archives: The palaeoenvironmental reconstruction of Zominthos (Central Crete), based on geophysical prospection, sedimentological investigations and GIS, Quatern. Int., 216, 75–92, https://doi.org/10.1016/j.quaint.2009.06.020, 2010.

Smith, G. H.: Test excavations in the oasis of Bir Abaruk, site 3, in: Qatar Archaeological Report – Excavations 1973, edited by: De Cardi, B., Oxford University Press, Oxford, UK, 26–34, 1978.

Sonnenfeld, P. and Perthuisot, J.-P.: Brines and Evaporites – Short Course Presented at the 28th International Geological Congress Washington, D.C. AGU, Washington, 126 pp., 1989.

State of Qatar (Ed.): Topographic map, 1 : 50 000, sheets 150/375 & 150/400, State of Qatar, Ministry of Public Works, 1971.

State of Qatar (Ed.): Geological map, 1 : 100 000, sheets 2–4, State of Qatar, Industrial Development Technical Centre, 1980.

Strohmenger, C. J. and Jameson, J.: Gypsum stromatolites from Sawda Nathil: relicts from a southern coastline of Qatar, Carbonate. Evaporite., 33, 169–186, https://doi.org/10.1007/s13146-017-0365-2, 2018.

Tetlow, E., Cuttler, R., Al-Naimi, F., Sheharyer, A., Bouhali, O., Delaney, L., and Adcock, J.: Landscape visualization, sea-level change, and human occupation in Wādī Debayān, north-western Qatar, Proc. Sem. Arab. Stud., 43, 337–348, 2013.

Tixier, J. (Ed.): Mission archéologique française à Qatar i, Ministry of Information, Doha, Qatar, 1980.

Uerpmann, M.: The Dark Millennium – Remarks on the Final Stone Age in the Emirates and Oman, in: Archaeology of the United Arab Emirates. Proceedings of the 1st International Conference on the Archaeology of the U.A.E., edited by: Potts, D. T., Al Naboodah, H., and Hellyer, P., Trident Press, London, UK, 73–84, 2003.

Uerpmann, M. and Uerpmann, H.-P.: Ubaid pottery in the eastern Gulf – new evidence from Umm al-Qaiwain (U.A.E.), Arab. Archaeol. Epigr., 7, 125–139, https://doi.org/10.1111/j.1600-0471.1996.tb00096.x, 1996.

Vita-Finzi, C.: Environmental History, in: Qatar Archaeological Report – Excavations 1973, edited by: De Cardi, B., Oxford University Press, Oxford, UK, 11–25, 1978.

Yechieli, Y. and Wood, W.: Hydrogeologic processes in saline systems: playas, sabkhas, and saline lakes, Earth Sci. Rev., 58, 343–365, https://doi.org/10.1016/S0012-8252(02)00067-3, 2002.

Yigiterhan, O., Alfoldy, B. Z., Giamberini, M., Turner, J. C., Al-Ansari, E. S., Abdel-Moati, M. A., Al-Maslamani, I. A., Kotb, M. M., Elobaid, E. A., Hassan, H. M., and Obbard, J. P.: Geochemical composition of Aeolian dust and surface deposits from the Qatar Peninsula, Chem. Geol., 476, 24–45, https://doi.org/10.1016/j.chemgeo.2017.10.030, 2018.

Supplement of E&G Quaternary Sci. J., 68, 215–236, 2020
https://doi.org/10.5194/egqsj-68-215-2020-supplement

Open Access E&G Quaternary Science Journal

Supplement of

Sediment-filled karst depressions and *riyad* – key archaeological environments of south Qatar

Max Engel et al.

Correspondence to: Max Engel (max.engel@uni-koeln.de)

S1 Methodological details of the magnetometer prospection

For our purpose to reach the highest possible sensitivity, a maximum speed of prospection and to get additional information on the enrichment of magnetic minerals in lateral sediments layers we chose the Cs total field magnetometer (Scintrex SM4G-Special). We applied the instrument by the so-called "duo-sensor" configuration. By this configuration, probes are mounted on a wooden frame and carried in zigzag-mode c. 30±5 cm above the ground (Fig. S11). The profiles of the 40 mx40 m grids were oriented E–W in order to minimize technical disturbance and interactions of the magnetometer probes with the electronic parts and the batteries of the device. The sampling frequency of the magnetometer (10 readings per second) allows the survey of a 40 m profile in less than 30 s, maintaining the spatial resolution of data sampling (10 measurements per second) of approximately 10–15 cm by normal walking speed. Every 5 m, in parallel to the magnetic data, a manual switch sets a marker. This helps to perform the best and most exact interpolation of data during the subsequent processing work, where we remove the slight linear changes in the daily variation of the geomagnetic field by a reduction filter and calculate the mean value of the 40 m profile. Additionally, we calculate the mean value of all data of the grid and subtract this value from the survey data. Hereby, we assume that the variation of the Earth's magnetic field during the measurement of one 40 m profile follows a linear increase or a linear decrease of the intensity of the Earth's magnetic field. Thus, it is possible to eliminate this variation for each traverse line by a reduction to the mean line value. Alternatively, in magnetically quiet areas, it is also useful to calculate the mean value of the whole 40 m×40 m grid and use this value for further data processing as described above. To create discrete field values we apply a resampling program setting the data to a sampling interval of 25 cm×25 cm. Additionally, by using this procedure, the difference between the measurement of both the magnetometer probes and the theoretically calculated mean value of the Earth's magnetic field is obtained. This intensity difference shows the apparent magnetic anomaly, caused by the magnetic properties of specific subsurface structures, the soil magnetism and the geology. The application of the optical pumped Cs magnetometer Smartmag in the duo-sensor configuration allows to set the reference value, e.g. the virtual gradient of the Earth's magnetic field, to infinity in order to enable recording of the full intensity of the magnetic anomalies (Fassbinder, 2015, 2017).

The great advantage of this configuration (compared to fluxgate gradiometers) is rather obvious. The resulting data not only provide a higher magnetic intensity of the anomalies and, hence, more information on the buried features, but also on deeper parts of magnetically enriched layers, ash layers, palaeo-channels, archaeological structures and changes in depositional environments. The SM4G-Special magnetometer measures the total Earth's magnetic field intensity by an intrinsic sensitivity of ±10.0 pT with a sampling rate of ten measurements per second. For comparison: The daily fluctuations of the Earth's magnetic field in Asaila (02/2014) varied within the range of c. 43510±20 nT.

The data were stored as binary files on the read-out unit, then downloaded to a Panasonic Toughbook and unpacked to ASCII data. For image processing and further treatment of the data (resampling), we applied a special self-made software, the program Geoplot (Geoscan Ltd. UK) and Surfer (Golden Software, USA). The visualization as a grey scale image (magnetogram) permits to trace even negligible anomalies originating from the shade of slightly enriched sediment layers beneath the surface. The

application of a high-pass filter removes the deeper and mainly geological features and provides supplemental information on the type of the anomalies. The magnetometer measurements were complemented by magnetic susceptibility measurements on the topsoil and rocks on the site, conducted using a handheld magnetic susceptibility meter SM-30 by ZHinstruments.

S2 Methodological details and results of the optically stimulated luminescence dating

Samples were taken from closed sediment cores (QAT 63), which were opened in dark conditions under subdued red light at the Cologne Luminescence Laboratory (CLL), and a trench (QAT 41), where thick-walled, opaque PVC tubes were carefully hammered into the trench wall. Water content for the samples was either calculated as maximum pore water content for samples that were identified to be located below the groundwater table during the entire period after deposition (QAT 63-3), or measured after sampling for samples clearly above the present groundwater table (QAT 63-1); for QAT 63-2 both values were used to calculate minimum and maximum dose rates, since the sample has been and is currently affected by water-level variations. U, Th, and K contents of the samples were determined by means of high-resolution gamma spectrometry. Dose rates were calculated with the dose rate and age calculator (DRAC) software (Durcan et al., 2015) using the conversion factors of Guérin et al. (2011) and the contribution of cosmic radiation according to Prescott and Hutton (1994). Minimum and maximum dose rates for QAT 63-2 are based on measured and saturated water contents, respectively. Samples for burial dose determination were processed under subdued red light following standard procedures to extract coarse-grain quartz. Samples were sieved to fractions of 100–200 µm, and treated with HCl (10%) and H_2O_2 (10%) to remove carbonates and organic matter. Density liquid was used to separate quartz grains from feldspar and heavy minerals (2.62<quartz<2.68 g/cm³). The alpha radiation-affected rim of the quartz grains and remaining feldspar contamination were removed by a final HF etch (40%) for 40 minutes. Large aliquots (8 mm diameter) of pure quartz grains were fixed on stainless steel discs using silicon spray. All dose measurements were performed on a Risø TL/DA 20 luminescence reader following a standard SAR (single aliquot regenerative dose) protocol (Murray and Wintle, 2003) with signal stimulation for 40 seconds using blue LEDs and signal detection through U340 filters. Preheat temperatures of 220–240 °C were experimentally determined by means of preheat-plateau tests (Fig. S1). Adequate performance of the protocol was evaluated on the basis of dose-recovery experiments (mean dose-recovery ratios of 0.95 to 1.01 for all samples; Fig. S2) and fitting of quartz signal components (all samples are dominated by the fast component; Fig. S3). A total of 20–47 aliquots per sample passed the acceptance criteria in terms of recycling ratio (0.9–1.1) and recuperation (<5% of the equivalent dose). Since the shape of the equivalent dose (De) distributions (Fig. S4) and over-dispersion values of 9–24% point to more or less complete signal resetting for all samples, burial doses were calculated using the central age model (Galbraith et al., 1999). Dose rates, burial doses and ages of all samples are compiled in Table S1.

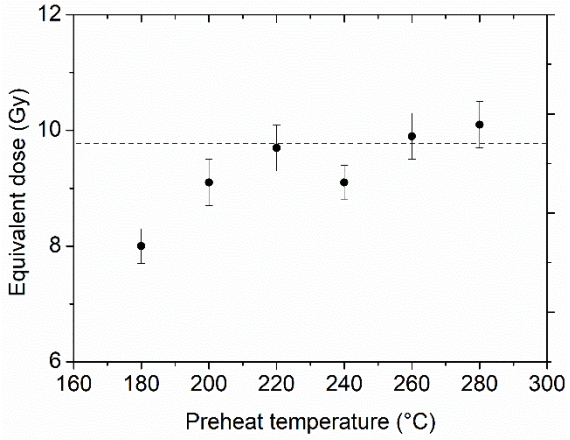

Fig. S1: Preheat-plateau test for sample QAT 63-2. Equivalent doses were determined with increasing preheat temperatures between 180 and 280 °C using four aliquots per temperature step. The mean equivalent doses form a plateau (blue dotted line) that indicates independence of thermal treatment for the temperature range 220–280 °C.

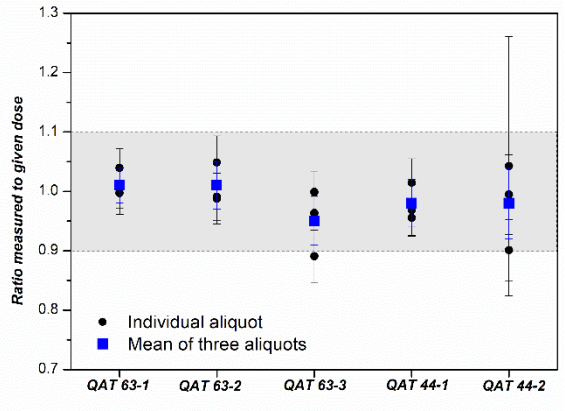

Fig. S2: Dose-recovery experiments for all samples. Three aliquots of each sample were bleached at room temperature with blue LEDs for 100 seconds, irradiated with a laboratory dose approximately equalling the burial dose, and measured using a standard SAR protocol. The mean dose-recovery ratios of all samples (blue squares) are in the acceptable range of 0.9–1.1.

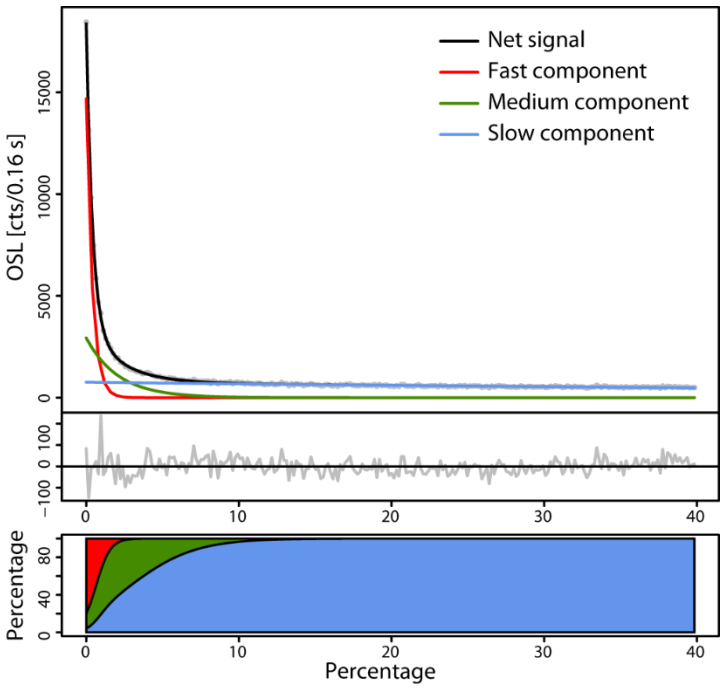

Fig. S3: Continuous wave OSL curve fitting for sample QAT 63-1. The first seconds of the quartz OSL signal, which are used for equivalent dose determination, are clearly dominated by the thermally stable and rapidly resetting fast component (red).

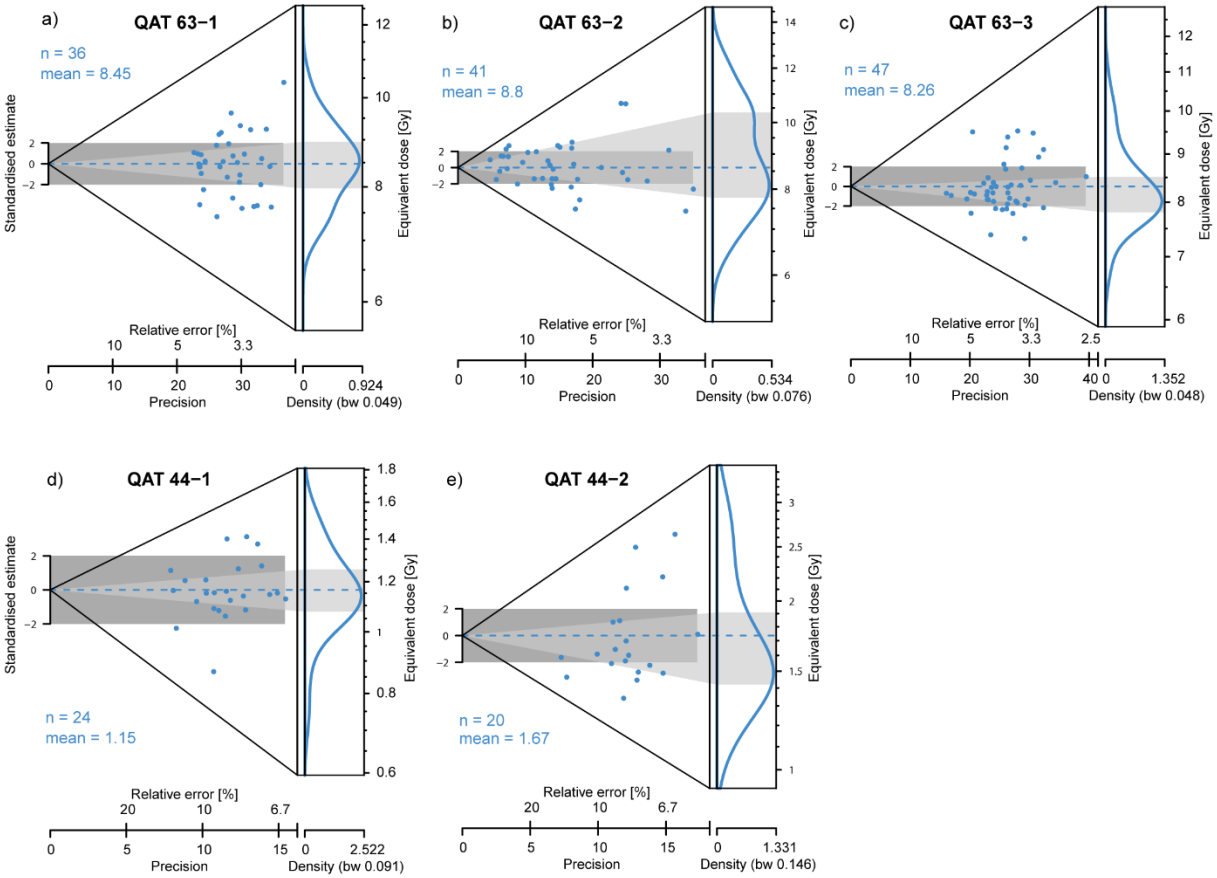

Fig. S4: Equivalent dose distributions of all samples shown as abanico plots.

Table S1: Compilation of OSL data for all five samples (DR_{tot}=environmental dose rate; n=number of accepted aliquots; OD=over-dispersion; De=equivalent dose). Measurements were carried out in the Cologne Luminescence Lab (CLL; lab code: C-L). Note that luminescence ages always refer to the year of sampling, in this case 2014. [1]For sample QAT 63-2, both measured and saturation water content were used for dose rate and age calculation.

Sample code	Lab code	Depth (m b.s.)	Grain size (µm)	U (ppm)	Th (ppm)	K (%)	Water (mass-%)	DR_{tot} (Gy/ka)	n	OD (%)	De (Gy)	Age (years)
QAT 63-1	C-L3937	0.50	150-200	0.84± 0.05	1.26± 0.11	1.07± 0.02	7±5	1.45± 0.06	36	8.8± 0.4	8.46± 0.14	5810±260
QAT 63-2	C-L3938	1.75	150-200	0.96± 0.05	1.43± 0.12	1.01± 0.02	10±5[1]; 25±5	1.19± 0.04[1]; 1.36± 0.06	43	15± 0.9	8.68± 0.25	6397±320[1]; 7293±338
QAT 63-3	C-L3939	2.75	150-200	0.76± 0.05	1.21± 0.11	0.98± 0.02	25±5	1.10± 0.04	47	8.6± 0.3	8.27± 0.12	7506±294
QAT 44-1	C-L4478	0.30	100-200	1.23± 0.07	2.02± 0.13	1.00± 0.02	2±5	1.63± 0.04	24	12± 2.6	1.16± 0.04	709±29
QAT 44-2	C-L4477	0.60	100-200	1.24± 0.06	2.02± 0.13	0.81± 0.02	2±5	1.42± 0.04	20	24± 4.3	1.68± 0.10	1182±75

S3 XRD spectra and sample locations

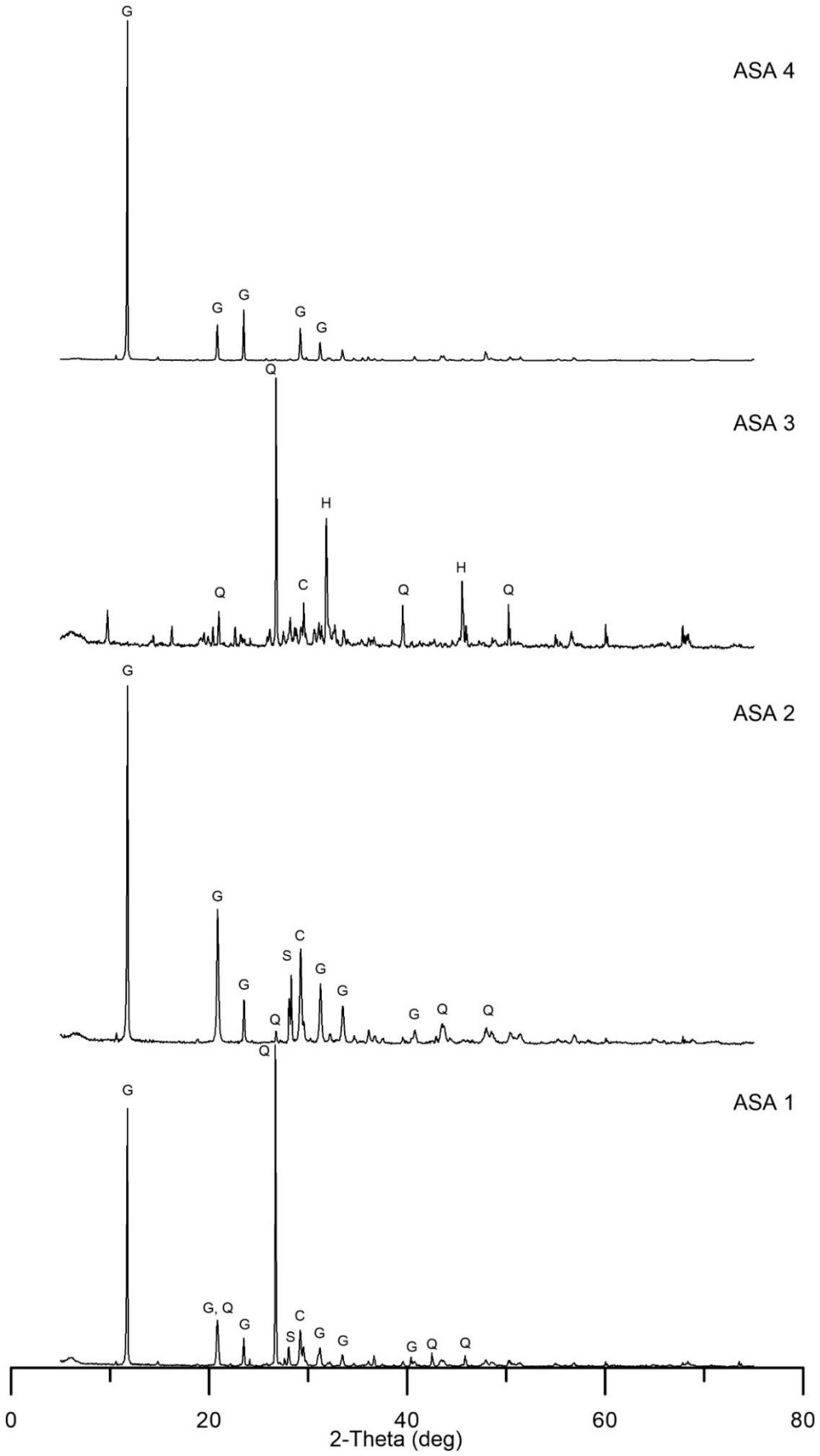

Fig. S5: XRD spectra of surface samples ASA 1–4 (Q=quartz; C=calcite; G=gypsum; H=halite; S=sylvine).

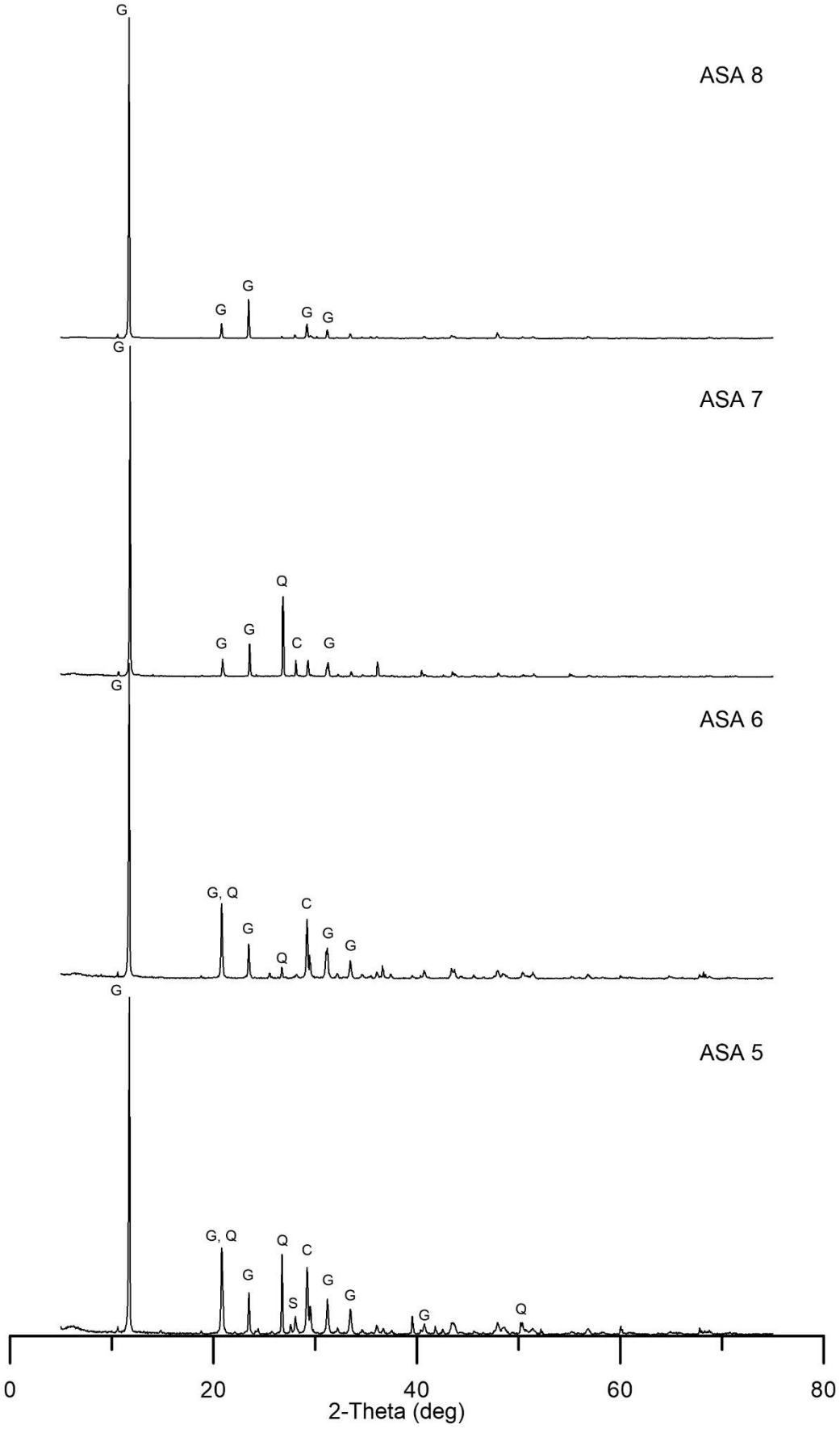

Fig. S6: XRD spectra of surface samples ASA 5–8 (Q=quartz; C=calcite; G=gypsum; S=sylvine).

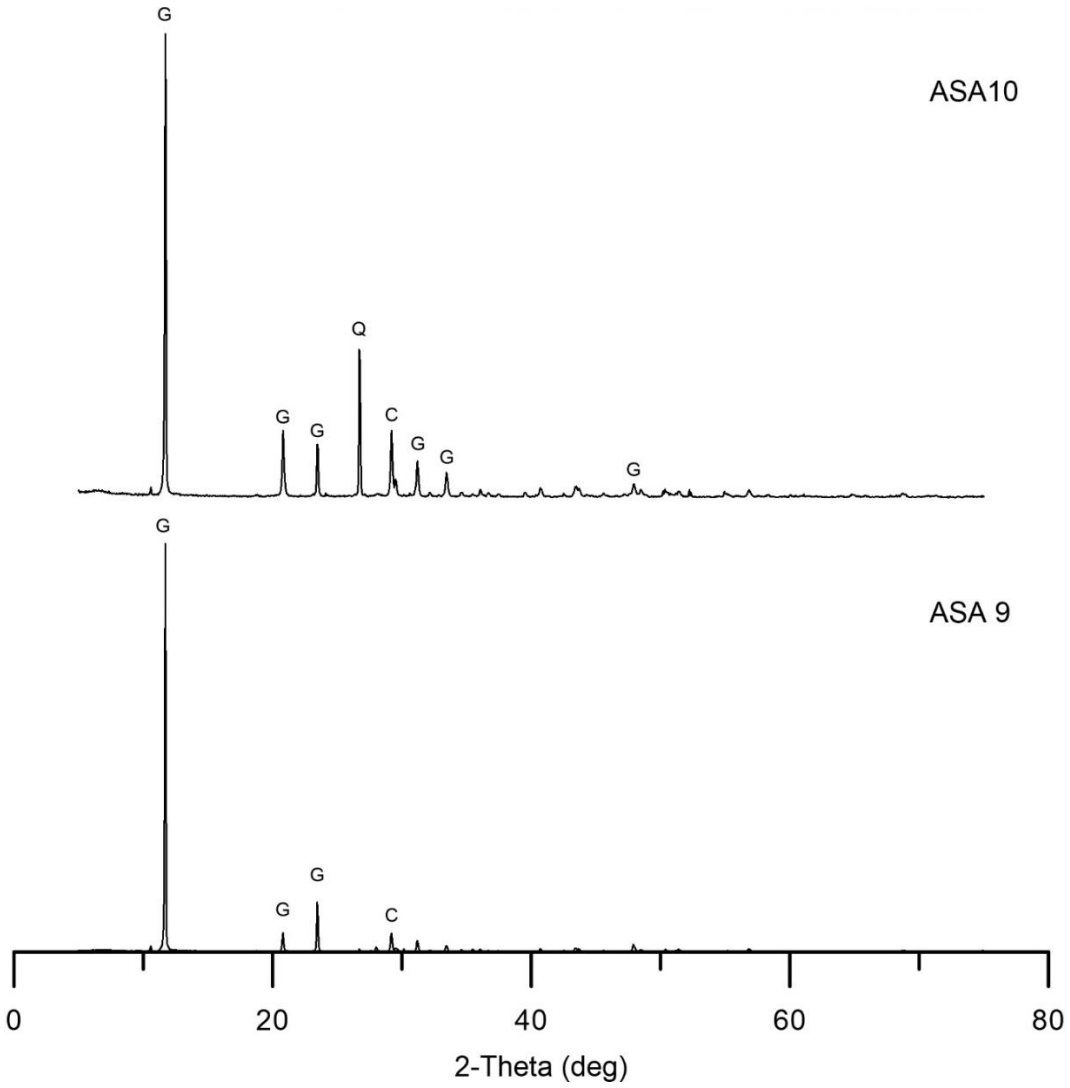

Fig. S7: XRD spectra of surface samples ASA 9 and 10 (Q=quartz; C=calcite; G=gypsum).

Table S2: Location and remarks for surface XRD samples (see Figs. 1, S5–S7).

Site	E	N	Geomorphic unit	Comp	
ASA 1	50.917740	25.2945961	Hummocky sand flats	G,Q,C,S	Relic evaporite crust of a low mound
ASA 2	50.921448	25.2966901	Hummocky sand flats	G,Q,C,S	Thick relic evaporite crust of a low mound
ASA 3	50.918090	25.2942141	Hummocky sand flats	G,Q,C,H	Active gypsum horizon; platy desert roses
ASA 4	50.917730	25.2940301	Hummocky sand flats	G	Pure gypsum crystals from root pseudo-morphs (gypsum precipitated around former rootlets) found at the surface.
ASA 5	50.915290	25.3000181	Round to elongated mounds (northern occurrence)	G,Q,C,S	White, porous, calcite-bearing gypsum from a rather low mound
ASA 6	50.915290	25.3000181	Round to elongated mounds (northern occurrence)	G,Q,C	Similar to ASA 5
ASA 7	50.916878	25.2969381	Wadi channel	G,Q,C	Reddish brown crust, 1-2 cm thick, few larger clasts at the surface
ASA 8	50.911465	25.2816721	Round to elongated mounds (southern occurrence)	G	Thick, relic crust, surface part
ASA 9	50.911465	25.2816721	Round to elongated mounds (southern occurrence)	G,C	Thick, relic crust, bottom part
ASA 10	50.912037	25.2851561	Linear mounds	G,Q	Relic, gypsum crust protecting linear features

S4 Geomorphic mapping of the Asaila basin: Systematic description of the landform units (Fig. 2)

S4.1. Higher limestone plateau (c. 13–18 m QVD[1])

The Asaila basin is surrounded by the flint-bearing limestone plateaus of the Dammam Formation. These plateaus are covered by a dense hamada surface comprising eroded remnants of *in-situ* limestone and flint (Figs. 3a, S8). The highest flint concentration can be found on the southern plateau, where numerous flint knolls outcrop at the surface, while it is lowest on the eastern plateau, where also the amount of finer material at the surface is higher and, thus, vegetation denser. *Stipa capensis* grass dominates the higher plateaus, while towards the slopes *Zygophyllum qatarense* and *Lycium shawii* occur. The slopes are mostly steep (>35°) to moderately steep (15–35°).

S4.2. Rugged higher limestone plateaus, ridges and buttes (c. 8–15 m QVD)

Towards the basin, the higher limestone plateaus merge into the more dissected, rugged higher limestone plateaus, ridges and buttes. This unit is present all along the basin margin and comprises iconic outliers protruding into the middle limestone plateaus and the basin itself (Figs. 3a, S9). The slopes are mostly moderately steep (15–35°) and covered by slope debris and aeolian sand. Besides the hamada, evaporitic crusts may appear at the surface, in particular in the north. Vegetation density is higher compared to the higher plateau and is dominated by the shrubs *L. shawii* and *Z. qatarense*, *Sclerocephalus arabicus*, as well as grasses *S. capensis* and *Panicum turgidum*.

S4.3. Lower limestone plateau (c. 2–8 m QVD)

Between the higher plateau and the bottom of the depression, there is a distinct plateau level formed by Dammam limestone (Figs. S10–S13), which only in the northeast gives way to a gentle slope (Fig. S10a). In the east, southeast, south and west, the lower limestone plateau is separated from the slopes leading towards the bottom of the depression by a clear topographical step of 1–2 m. It is mostly covered by hamada (Fig. S8), in some parts consolidated by an evaporitic crust. Vegetation is relatively dense and dominated by grasses, while occasional *Acacia tortilis* trees can be found.

S4.4. Terraced slope debris

The slopes of the middle limestone plateaus towards the depression are covered by multimodal slope debris that mainly result from a combination of aeolian sand sedimentation and the gravitational deposition of larger clasts (Fig. 3a). Large limestone clasts characterize the low-inclination surface (2–7°). Vegetation is very sparse.

S4.5. Sand ramps

Along the northeastern margin, short ramps of unimodal sand are being accumulated basinward on top of the slope debris, extending from the edge of the higher and lower limestone plateaus where they may also cover the southern to southeastern slopes of the outliers (Figs. S9, S12). Sand is supplied from locations in the north and delivered by the Shamal wind system. Sand grains saltating over the plateaus and passing their edges feed the ramps as the abrupt topographical change reduces aeolian

[1] QVD = Qatar Vertical Datum, defined as the mean sea level 1970–1972; reference mark located at the old airport of Doha

transport competency. Narrowly spaced wind ripples indicate that the sand ramps are actively forming, which prevents the establishment of vegetation. In some places, the sand ramps are covered by collapsing caprock (Fig. S10b).

S4.6. Gravel sheets

The transition area between the terraced slope debris and the bottom of the depression is occupied by a sand and fine gravel cover with a low concentration of larger clasts (coarse cobbles to fine boulders) (Figs. 3a, S11, S13). It differs from the hamada on the higher limestone plateau in terms of their high percentage of sand. The gravel sheets gently incline towards the center of the depression. Where evaporitic crusts occur at the surface, the gravel sheet forms a terrace with a clear basinward step. Vegetation is very sparse, similar to the terraced slope debris units.

S4.7. Hummocky sand flats

The gravel sheets often merge into a sand flat with active aeolian dynamics (Fig. S13), indicated by *Z. qatarense* shrubs forming a wide range of sand accumulations from small, narrow and crested leeward dunes up to substantial nebkhas (Figs. S14, S15). These hummocky sand flats cover the major part of the depression. In some cases, the sandy mounds are consolidated by evaporitic crusts, have grown beyond single-shrub-centred nebkha size, and their morphodynamic activity is reduced. Surface samples ASA 1 and 2 show that the crust is made up of gypsum, quartz sand, calcite and minor occurrences of sylvine, an easily soluble salt (Fig. S5, Table S2). In some places, gypsum-based root pseudomorphs (surface sample ASA 4; Fig. S5, Table S2) were found at the surface (Fig. S16), indicating predominant deflation, and in some areas desert roses (platy, circular crystal clusters of gypsum and quartz sand, with minor incorporation of calcite and halite as indicated by surface sample ASA 3; Fig. S5, Table S2) grow actively (Figs. S17, S18). Besides the dense cover of *Z. qatarense*, the hummocky sand flats, comprise grasses such as *P. turgidum* and *Cistanche tubulosa*.

S4.8. Sabkha-type sand flats

The northwestern and southwestern parts of the depression, characterized by the lowest elevations, comprise sandy, vegetation-free areas with flat, salt- and gypsum-encrusted, sabkha-type surfaces, some even with halite-containing polygonal patterns at the surface (Figs. 3a,b, S19, S20). These are the areas of highest moisture and appear darker in the satellite images (e.g., Fig. S9d).

S4.9. Round to elongated mounds

In particular in the central southern areas of the Asaila basin, mounds of varying shape and density occur. Their uppermost part is consolidated by evaporitic crusts. The mounds vary from perfectly round, up to 1 m high, to narrow ridges, several tens of metres long (Fig. 3b, S21). Vegetation is generally less dense compared to the hummocky sand flats and mainly comprises *Z. qatarense and Aizoon canariense*. The unit has three different subtypes:

(a) Linear ridges in the southwestern basin, partly cross-cutting, with seemingly random orientation (Fig. S21). In between the ridges, active aeolian deposition occurs. Here, the crust is rather porous, white to light grey and mostly several centimetres thick; surface sample ASA 10 contains gypsum and quartz (Fig. S7, Table S2).

(b) Round to more elongated, often yardang-type mounds with a long axis aligned to the Shamal corridor (Fig. S22, S23). Active aeolian deposition occurs in between the mounds. The evaporitic crust protecting the mounds is relatively thick (up to 30–40 cm). Its texture ranges from massive (Figs. S25, S26) to porous (Figs. S27, S28) gypsum (surface samples ASA 5, 6, 8, 9), with contributions of quartz sand and calcite (ASA 5, 6, 9), and, only very occasionally, sylvine (ASA 6 [Figs. S6, S7, Table S2]). Boundaries between (a) and (b) may appear gradual.

(c) Lower density of mounds and only thin, sometimes even absent evaporitic crusts and reduced vegetation cover; the area shares some similarities with and also merges into the sabkha-type sand flats. Some active aeolian deposition occurs in between the mounds (Fig. S24).

S4.10. Wadi and channel

Two areas inside the basin exhibit unequivocal signs of surface water flows. Extending from the central northern margin and bifurcating towards the centre of the basin is a vegetation-free, linear depression of 10–20 cm (Fig. 5) with a weak, reddish-brown surface crust of gypsum, quartz sand and calcite (Fig. S6, Table S2) with high amounts of clay and silt (Fig. S31).

The eastern end of the Asaila basin is characterized by retrogressive erosion associated with a wadi channel (Figs. S29, S30). The wadi is filled with slope debris and experiences aeolian overprinting in the form of sand ramps (Figs. S12, S29a). However, horizontally bedded platy clasts in a poorly sorted, consolidated sandy matrix and an outwashed channel exposing barren bedrock point to at least episodic surface water flows (Figs. S29a, S30a). Vegetation is dense comprising *A. tortilis* und *L. shawii*.

S4.11. Areas of modern land use

Besides dirt roads and single tracks crossing the depression, temporary camel and sheep farms are set up in the Asaila basin. At the entrance of the southeastern wadi, a permanent date farm was installed in the 1970s, fed by artificial wells, which is today abandoned (Gerber et al., 2014). North of the date farm, the remains of the Islamic Asaila Fort (Hardy-Guilbert, 1980) are located on an outlier of the higher limestone plateau.

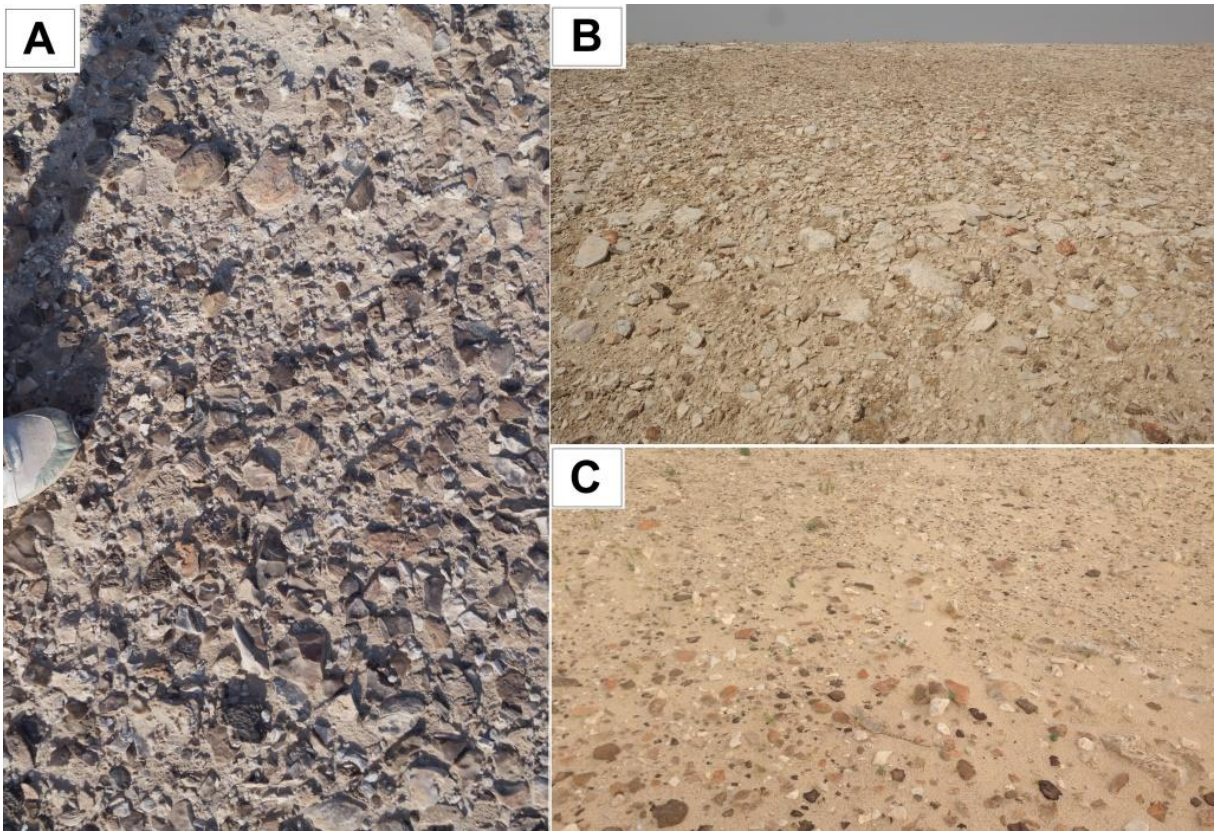

Fig. S8: Typical hamada surfaces of the higher and lower limestone plateaus north (A) and east (B,C) of the Asaila basin.

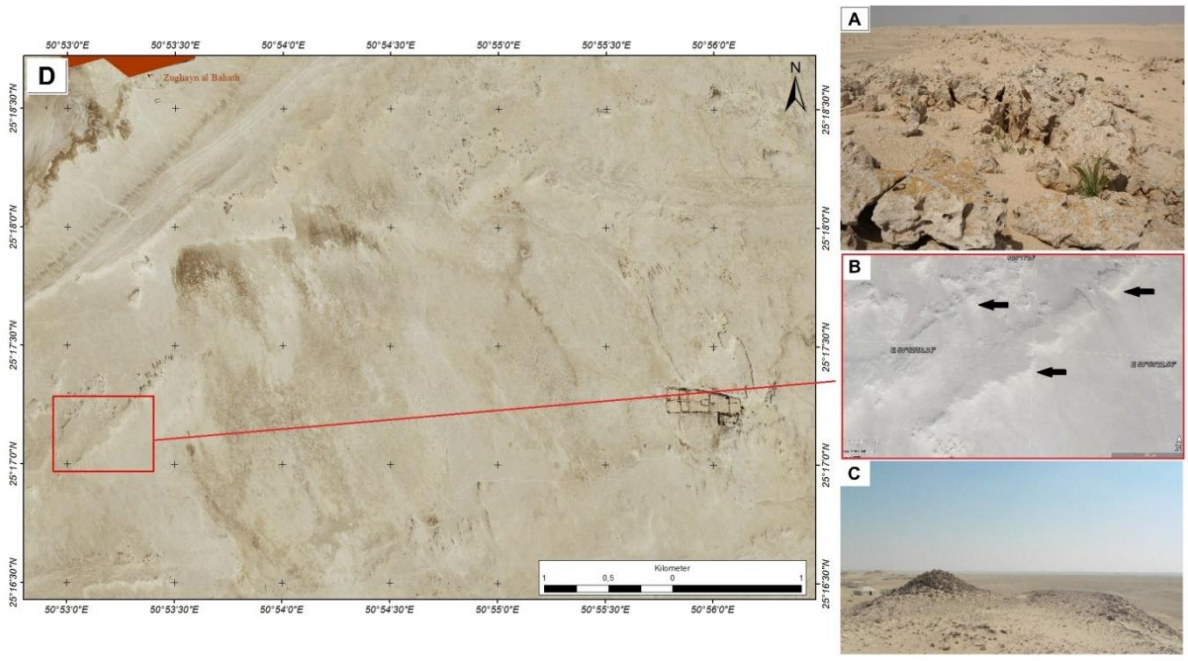

Fig. S9: Rugged higher limestone ridge as part of the plateau unit at the western margin of the Asaila basin (A,D [IKONOS imagery 2004]), with sand ramps along the southeastern edge (light areas in B; Google Earth), where sands driven by the Shamal winds and saltating over the plateau lose support by the wind. (C) Outliers of the higher plateau with evaporitic cementation.

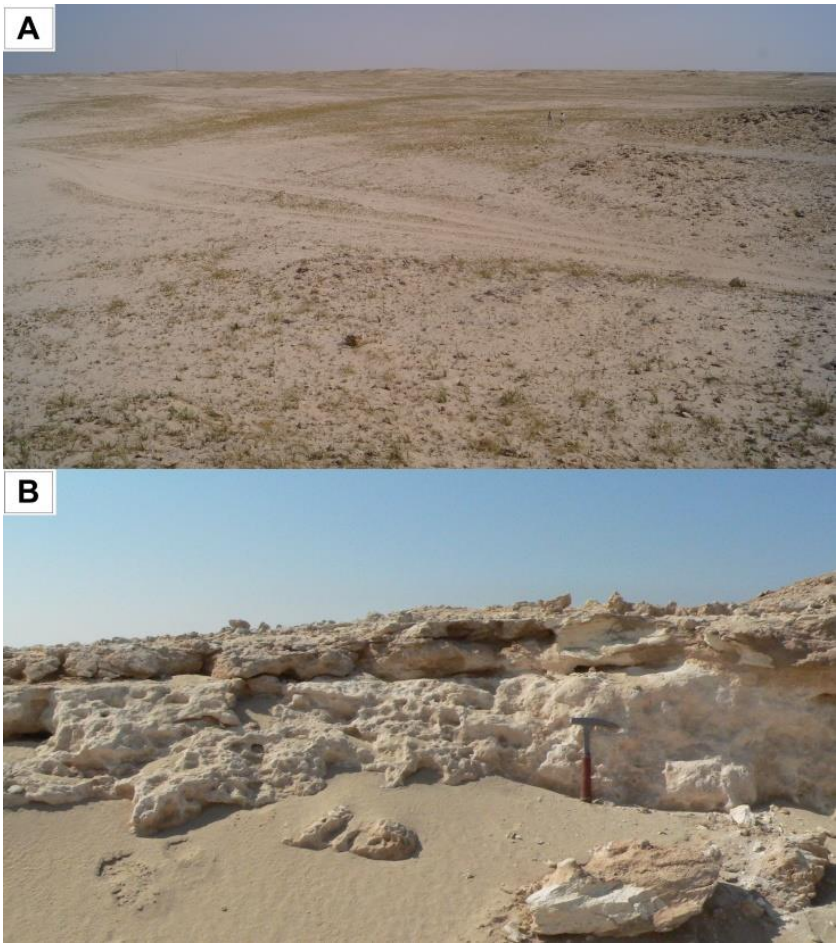

Fig. S10: Different aspects of the lower limestone plateau. (A) View over the area of the magnetic prospection (Figs. 2,4) with the smoothly inclined surface towards the basin created by multimodal, sand-dominated deposition covering the limestone plateau (very similar to the adjacent gravel sheets). (B) Lower Dammam limestone forming the lower limestone plateau in the west of the Asaila basin; the cliff framing the basin is typically masked by a sand ramp.

Fig. S11: Magnetometer prospection (Figs. 2,4) in the environs of the old Acila 36 excavation of Inizan (1988) and Pelegrin and Inizan (2013), at the transition of the incised and sediment-filled lower limestone plateau (densely covered by grasses) and the gravel sheet.

Fig. S12: Sand ramps accumulated against the cliff of the lower limestone plateau in the wadi area of the western Asaila basin.

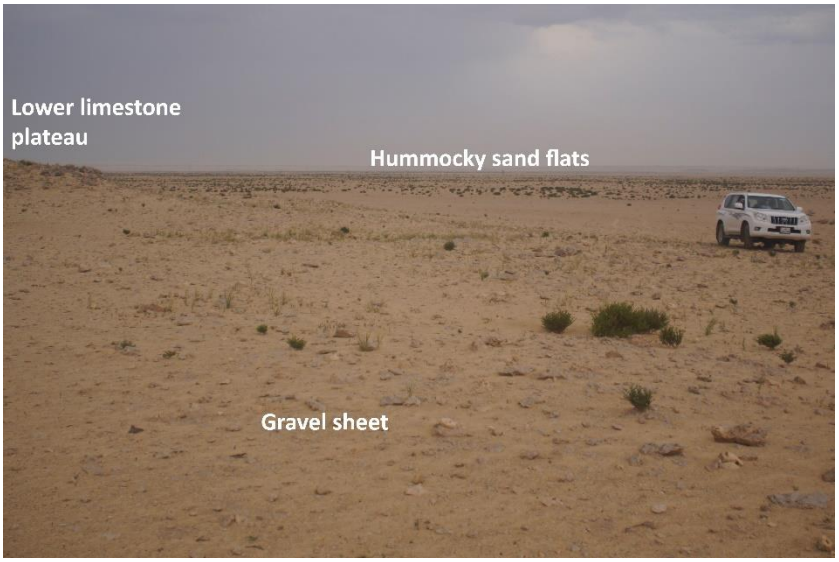

Fig. S13: Transition between the gravel-dominated sheets and hummocky sand flats of the inner basin at the northwestern margin of the Asaila basin, downslope of the magnetometer prospection area (Fig. 2).

Fig. S14: Nebkha field as part of the hummocky sand flat in the centre of the Asaila basin.

Fig. S15: Sand tail (or proto-nebkha) downwind of a *Zygophyllum qatarense* shrub inside the hummocky sand flats.

Fig. S16: Root pseudomorphs: pure gypsum precipitated around former rootlets (cf. sample ASA 4 in Fig. S5 and Table S2). The fact that they are now exposed and distributed over the surface indicates a predominant deflation regime.

Fig. S17: Desert roses actively growing 20 cm below the surface of the hummocky sand flats.

Fig. S18: Zoom into the horizon of desert roses (up to c. 7–8 cm large plates).

Fig. S19: Sabkha-type sand flats, in some areas showing polygonal surface patterns induced by active halite, carbonate and gypsum precipitation.

Fig. S20: Coring site QAT 63 on the sabkha-type sand flats.

Fig. S21: Linear, crosscutting mounds in the central southern Asaila basin (subtype a in Fig. 2).

Fig. S22: Small field of rounded mounds (subtype b in Fig. 2) in the central northern Asaila basin, merging into the hummocky sand flats, rich in *Z. qatarense*.

Fig. S23: Elongated to rounded mounds in the central southern Asaila basin (subtype b in Fig. 2).

Fig. S24: Lower-density mound field (subtype c in Fig. 2) with very sparse vegetation cover and active aeolian deposition.

Fig. S25: Elongated to rounded mounds in the central southern Asaila basin with moderate vegetation (subtype b in Fig. 2).

Fig. S26: Zoom into the profile in Fig. S25 showing the typical white, relict gypsum crust of c. 15 cm thickness preserving the mounds.

Fig. S27: Profile in rounded mound field of the central northern Asaila basin with thinner, more porous gypsum crust (subtype b in Fig. 2).

Fig. S28: Zoom into the profile of Fig. S27 showing a thinner, more porous and calcite-bearing version of the white gypsum crust preserving the mounds.

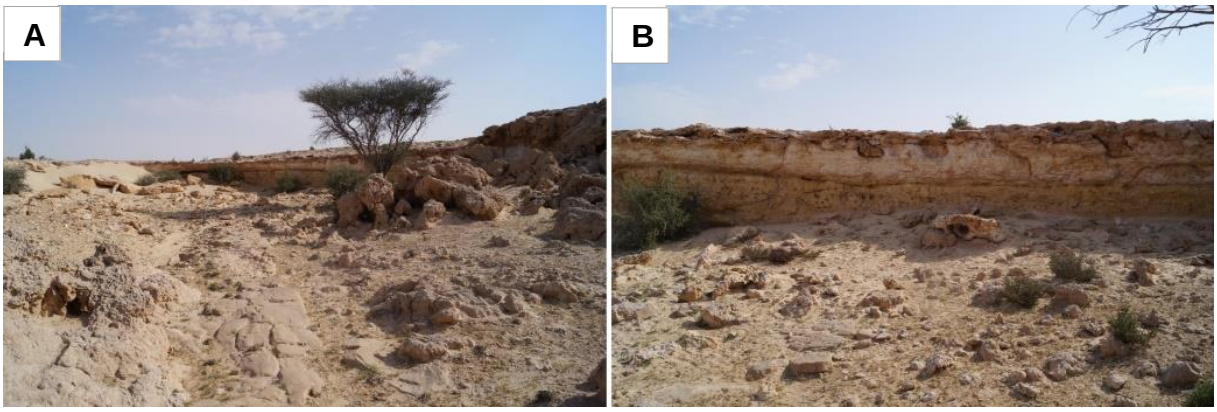

Fig. S29: Wadi of the eastern Asaila basin with traces of recent surface runoff exposing the bedrock in the central prt of the picture (A). While downwind of the Shamal, relatively pure sand ramps develop (left background of A), most steep flanks are covered by gravitational talus slopes (B).

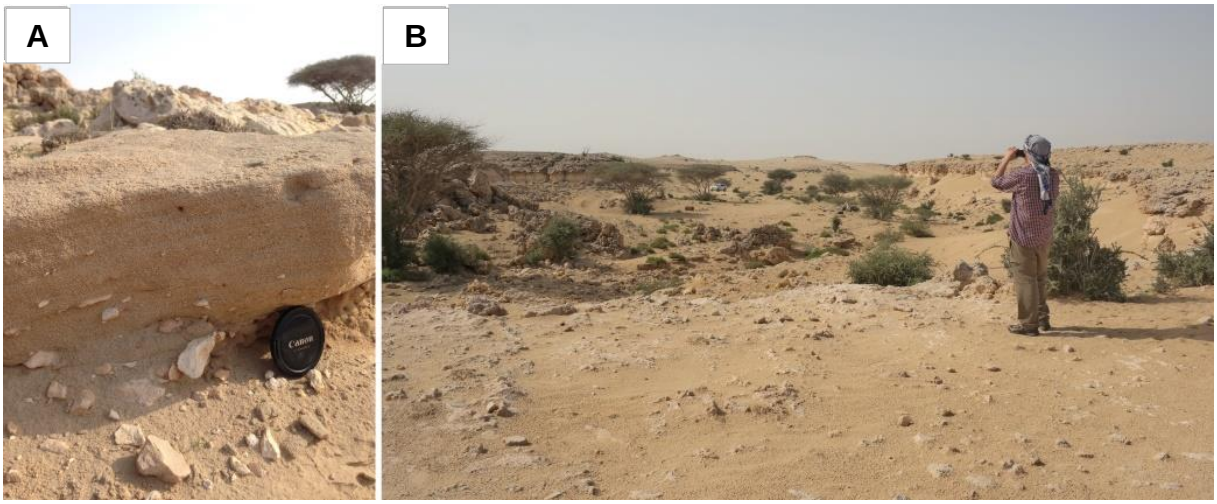

Fig. S30: Laminated bedding of poorly sorted facies with parallel aligned limestone clasts resulting from episodic fluvial activity inside the wadi. The deposit is modern, but weakly cemented by carbonate (A). (B) Overview from the wadi head.

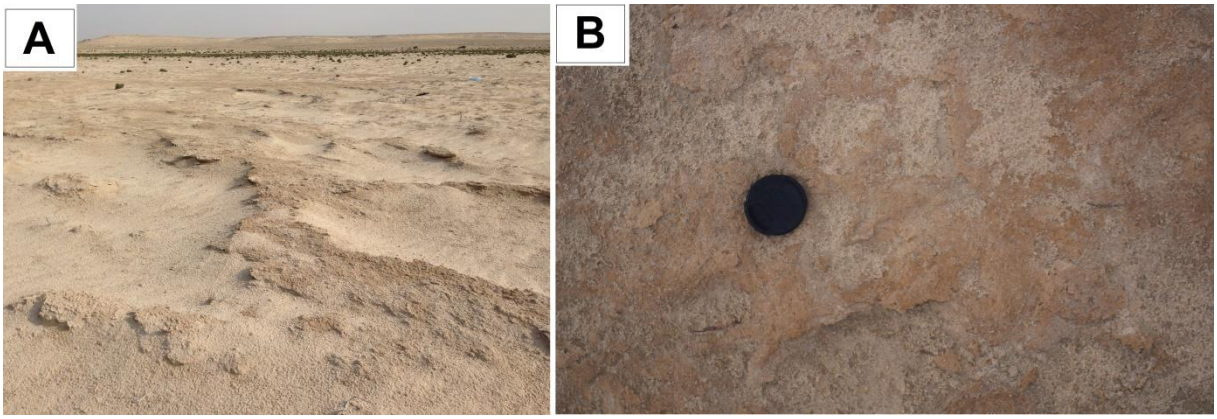

Fig. S31: Shallow, vegetation-free wadi channel (A) with thin, fragmented, reddish brown surface crust (B) entering the Asaila basin in the north (Fig. 5).

Fig. S32: View towards the basin of Jaow Aqeeq from the eastern edge, with temporary standing water (upper left) and the sabkha area (dark brown, framing the water) in the background. The red arrow indicates coring site ASA-C1 (Fig. 7) in the sabkha area.

Fig. S33: Linear corrasion features on a rawdha surface of southern Qatar. The arrow indicates the main Shamal direction (Engel et al., 2018).

Fig. S34: Micro-yardang (long axis <50 cm) inside a rawdha of southern Qatar indicating active deflation mainly induced by the Shamal (white arrow shows the yardang's long axis and the dominant wind direction). Its formation is supported by protection of a small boulder, while the surrounding surface has been lowered by deflation (Engel et al., 2018).

References

Durcan, J. A., King, G. E., and Duller, G. A. T.: DRAC: Dose rate and age calculator for trapped charge dating, Quat. Geochronol., 28, 54–61, doi:10.1016/j.quageo.2015.03.012, 2015.

Engel, M., Boesl, F., and Brückner, H.: Migration of barchan dunes in Qatar—controls of the Shamal, teleconnections, sea-level changes and human impact, Geosciences, 8, 240, doi:10.3390/geosciences8070240, 2018.

Fassbinder, J. W. E.: Seeing beneath the farmland, steppe and desert soil: Magnetic prospecting and soil magnetism, J. Archaeol. Sci., 56, 85–95, doi:10.1016/j.jas.2015.02.023, 2015.

Fassbinder, J. W. E.: Magnetometry for Archaeology, in: Encyclopedia of Geoarchaeology, edited by: Gilbert, A. S., Springer, Dordrecht, 499–514, doi:10.1007/978-1-4020-4409-0_169, 2017.

Galbraith, R. F., Roberts, R. G., Laslett, G. M., Yoshida, H., and Olley, J. M.: Optical dating of single grains of quartz from Jinmium rock shelter, northern Australia, Part I: experimental design and statistical models, Archaeometry, 41, 339–364, doi:10.1111/j.1475-4754.1999.tb00987.x, 1999.

Gerber, C., Drechsler, P., Yasin-Meier, D., Brückner, H., Engel, M., Meier, D.M.P., Götzelt, T., Daitche, J., Hörwarthner, D., Lienig, A., Reising, R., and Tiltmann, S.: The German-Qatari South Qatar Survey Project: The 2012–2013 Season, Z. Orient Archäol., 7, 248–275, 2014.

Guérin, G., Mercier, N., and Adamiec, G.: Dose-rate conversion factors: update, Ancient TL, 29, 5–8, 2011.

Hardy-Guilbert, C.: Recherches sur la période islamique au Qatar, in: Mission archéologique à Qatar, tome 1, edited by Tixier, J., Doha, 111–128, 1980.

Inizan, M.-L. (Ed.): Préhistoire à Qatar. Mission archéologique française à Qatar (2), Éditions Recherche sur les Civilisations, Paris, France, 1988.

Murray, A. S., and Wintle, A. G.: The single aliquot regenerative dose protocol: potential for improvements in reliability, Radiat. Meas., 37, 377–381, doi:10.1016/S1350-4487(03)00053-2, 2003.

Pelegrin, J., and Inizan, M.-L.: Soft hammerstone percussion use in bidirectional blade-tool production at Acila 36 and in bifacial knapping at Shagra (Qatar), Arab. Archaeol. Epigr., 24, 79–86, doi:10.1111/aae.12016, 2013.

Prescott, J. R., and Hutton J. T.: Cosmic ray contributions to dose rates for luminescence and ESR dating: Large depths and long-term time variations, Radiat. Meas., 23, 497–500, doi:10.1016/1350-4487(94)90086-8, 1994.